American Mineralogist, Volume 94, pages 1085–1102, 2009

Bonded interactions in silica polymorphs, silicates, and siloxane molecules

G.V. Gibbs,[1,*] A.F. Wallace,[1] D.F. Cox,[2] R.T. Downs,[3] N.L. Ross,[1] and K.M. Rosso[4]

[1]Department of Geosciences, Virginia Tech, Blacksburg, Virginia 24061, U.S.A.
[2]Department of Chemical Engineering, Virginia Tech, Blacksburg, Virginia 24061, U.S.A.
[3]Department of Geosciences, University of Arizona, Tucson, Arizona 85721, U.S.A.
[4]Chemical and Materials Science Division, and the W.R. Wiley Environmental Molecular Sciences Laboratory, Pacific Northwest National Laboratory, Richland, Washington 99352, U.S.A.

Abstract

Experimental model electron density distributions obtained for the silica polymorphs coesite and stishovite are comparable with electron density distributions calculated for various silicates and siloxane molecules. The Si-O bond lengths and Si-O-Si angles calculated with first-principles density functional theory methods as a function of pressure are also comparable with the bond lengths and angles observed for coesite and quartz within the experimental error. The similarity of the topological properties of the Si-O bonded interactions and the experimental and the geometry-optimized structures for the silica polymorphs provide a basis for understanding the properties and crystal chemistry of silica. The agreement supports the argument that the bulk of the structural and physical properties of the silica polymorphs are intrinsic properties of molecular-like coordination polyhedra such that the silica polymorphs can be pictured as "supermolecules" of silica bound by virtually the same forces that bind the Si and O atoms in simple siloxane molecules. The topology of the electron density distribution is consistent with the assertion that the Si-O bonded interaction arises from the net electrostatic attraction exerted on the nuclei by the electron density accumulated between the Si and O atoms. The correlation between the Si-O bond length and Si-O-Si angle is ascribed to the progressive local concentration of the electron density in the nonbonded lone pair region of the O atom rather than to a bonded interaction that involves the *d*-orbitals on Si.

The accumulation of deformation electron density, $\Delta\rho(\mathbf{r})$, in the bonded and nonbonded regions of the Si-O bond, the close proximity of the bond critical point, $\mathbf{r}_c$, of the bond with the nodal surface of the Laplacian and the negative value of the total energy density are taken as evidence that the bond has a nontrivial component of shared character. For M-O bonded interactions for first and second row metal atoms bonded to O, $\nabla^2\rho(\mathbf{r}_c)$ is positive and increases linearly as $\rho(\mathbf{r}_c)$ and $G(\mathbf{r}_c)/\rho(\mathbf{r}_c)$ both increase and as the value of $H(\mathbf{r}_c)$ decreases; the greater the shared character of the interaction, the larger the values of both $\nabla^2\rho(\mathbf{r}_c)$ and $G(\mathbf{r}_c)/\rho(\mathbf{r}_c)$. In addition, a mapping of $\nabla^2\rho(\mathbf{r})$ serves to highlight those Lewis base domains that are susceptible to electrophilic attack by H, like the O atoms in coesite involved in bent Si-O-Si angles; the narrower the angle, the greater the affinity for H. On the basis of the net charges conferred on the Si and O atoms and the bonded radii of the two atoms, the Si-O bond for stishovite, with six-coordinated Si and three-coordinated O, is indicated to be more ionic in character than that in quartz with four-coordinated Si and two-coordinated O. Unlike the conclusion reached for ionic and crystal radii, it is the bonded radius of the O atom that increases with the increasing coordination number of Si, not the radius of the Si atom. The modeling of the electron density distributions for quartz, coesite, and beryl as a function of pressure suggests that the shared character of the bonded interactions in these minerals increases slightly with increasing pressure. The insight provided by the calculations and the modeling of the electron density distributions and the structures of the silica polymorphs bodes well for future Earth materials studies that are expected to improve and clarify our understanding of the connection between properties and structure within the framework of quantum mechanical observables, to find new and improved uses for the materials and to enhance our understanding of crystal chemistry and chemical reactions of materials in their natural environment at the atomic level.

Keywords: Bonded interactions, electron density distributions, silica, coesite, quartz, stishovite, cristobalite, siloxane

"While science is pursuing a steady onward movement, it is convenient to cast a glance back on the route already traversed, and especially to consider new conceptions which aim at discovering the general meaning of the stock of facts accumulated from day to day in our laboratories." Dmitri Mendeleeff (1889), Faraday Lecture delivered before the Fellows of the Chemical Society

Introduction

The concept of the chemical bond has played a pivotal role in advancing our understanding of the structures, properties, and reactivity of materials at the atomic level. Since the nineteenth century, interest in the concept has burgeoned as evinced by the large number of papers, review articles and books that have been written on the topic. For example, since Linus Pauling wrote his classic paper entitled "The nature of the chemical bond" in 1931, more than 26 000 papers have been published about one or more aspects of the concept, evidence of the profound impact that it has had on chemical thinking and research. It is generally accepted that a chemical bond is the result of the net electrostatic attraction exerted on the nuclei of a pair of atoms by the electron density (ED) accumulated between the nuclei (Feynman 1939). Nevertheless, given that a chemical bond is not a quantum mechanical observable, the famous mathemati-

* E-mail: ggibbs@vt.edu

0003-004X/09/0809–1085$05.00/DOI: 10.2138/am.2009.3215

cian Charles A. Coulson (1955) concluded, in a lecture delivered before the Royal Society, that "A chemical bond is not a real thing: it does not exist, no one has ever seen it, no one ever can. It is a figment of our imagination." Bader (2008) recently stated that "There are no chemical bonds, they simply don't exist, only bonded atoms exist." Hoffmann (1988) added that physicists do not see chemical bonds, they only see bands. But, Pauling (1939) wrote, in his famous book, *The Nature of the Chemical Bond*, that quantum mechanics has not only clarified the mystery that has shrouded the nature of the chemical bond, but it has also introduced into chemical theory the concepts of hybridization, resonance, bond character, and a set of rules for the formation of covalent and ionic bonds. But, as countered by Coulson (1953), "Concepts like hybridization, resonance, covalent, and ionic structures do not appear to correspond to anything directly measurable." It also appears that empirical concepts like ionic and crystal radii, bond strength, valence, and bond valence that have worked well for mineralogists and geochemists in the modeling of bond-length variations, properties, acid and base sites and structure likewise do not appear to correspond with anything that is directly measurable. In a recent discussion on the chemical bond quandary, Alvarez et al. (2009) observed that "Chemistry has done more than well in creating a universe of structure ... with just this imperfectly defined concept of a chemical bond. Or maybe it has done well precisely because the concept is flexible and fuzzy." Clearly, as asserted by the chemical physicist Robert Mulliken, the concept of "the chemical bond is not so simple as some people seem to think" (Coulson 1960). Given these inconvenient truths, Cremer and Kraka (1984) reiterated that "There is no way to measure a bond or any bond property." They continued by declaring that a bonded interaction can only be defined within the framework of a given model like Bader's (1990) topological model of the ED distribution, which provides a basis for defining a bonded interaction, bond strength, net atomic charges, and bonded radii for the atoms in molecules and crystals.

Overview

This report begins with an examination of the ED distribution that defines the Si-O bonded interactions for a siloxane molecule in terms of its bond paths, bonded radii, bond critical points, and the associated properties followed by an examination of the Laplacian of the ED distribution, an ideal tool for characterizing and locating Lewis base and acid domains, sites of potential electrophilic and nucleophilic attack, respectively. Next, the topological properties of the Si-O bonded interactions in several silica polymorphs and representative molecules are explored. The results show that the experimentally determined properties of the ED distributions are comparable with those calculated with first-principles quantum mechanical methods, and that model structures for selected framework silicates calculated as a function of pressure are comparable with those observed. A fundamental connection will be established between the topological properties of the ED distribution and Lewis base lone-pair domains on the oxide anions involved in Si-O-Si bonded interactions and the incorporation of water via the hydrogarnet substitution in the coesite structure at high temperatures and pressures. The correlation between the Si-O bond length and the Si-O-Si angle observed for coesite will be examined in terms of a progressive concentration of the ED in the anti-binding lone pair regions of the O atoms. It will be established that the bond critical point properties for the ED distributions calculated for a relatively large number of silicates vary systematically with the experimental Si-O bond lengths, providing a connection between bond length variation and the topological properties of the ED. Likewise, the properties of the bonded interactions for representative siloxane molecules will be shown to be comparable with the calculated and experimental trends in the topology of the ED distributions for the silicates. Together with Si-O bonded interactions, the value of $\nabla^2\rho(\mathbf{r}_c)$ for intermediate M-O bonded interactions (M = first and second row metal atoms bonded to O) in silicates will be examined in terms of the values of $\rho(\mathbf{r}_c)$. The character of the Si-O bond will also be re-examined in terms of a spectrum of bonding models, ranging from closed shell (ionic) to shared (covalent) bonded interactions. The ratio $\mathbf{G}(\mathbf{r}_c)/\rho(\mathbf{r}_c)$ will be examined in terms of the Si-O and M-O bond lengths and the coordination numbers for the Si and M atoms. Ionic and crystal radii, determined by assuming a given size for the oxide anion combined with the additive rule, are considered to be unreal and not measurable, unlike bond radii. The bonded radius of the oxide anion is observed to be highly dependent on the properties of the atoms to which it is bonded. The radii for the Si and O atoms involved in the bonded interactions for the silica polymorphs will be shown to differ from the crystal radii in the way that they respond to changes in coordination number and pressure. The report will conclude with a brief statement examining the connections that exist between the Si-O bonded interactions in crystals and molecules, bonded radii and bond critical point, and local energy-density properties, and the rewards that we believe will be forthcoming by the studying Earth materials and their properties in terms of their ED distributions with first-principle quantum mechanical methods.

Bader's topological model for electron density distributions

Given that there are no chemical bonds, only bonded interactions, Bader and his colleagues (Bader 1985; Runtz et al. 1977) undertook the challenge of probing the topology of the ED distribution in the region between the nuclei of adjacent atoms in a search for a feature that might qualify as an indicator of a bonded interaction. The ED was chosen for study because, unlike the chemical bond, it is a quantum mechanical observable (it is the expectation value of the density operator). It also follows that any property of the ED distribution, including the value of the ED, $\rho(\mathbf{r})$, the gradient field, $\nabla\rho(\mathbf{r})$, and the Laplacian of $\rho(\mathbf{r})$, $\nabla^2\rho(\mathbf{r})$, at a given point $\mathbf{r}$ and the bond lengths and angles of a molecule or crystal, are also observables. In addition, the ED distribution is a robust property that embodies all of the information that can be known about a ground state material, including its kinetic, potential, and total energies (Parr and Yang 1989). Moreover, the distribution adopted by a system at equilibrium (a system in which there are no net forces acting on the nuclei) is one that results in the lowest net energy for the system as a whole (Gatti 2005). In the analysis of the ED distribution, it was discovered that adjacent atoms in molecules are often connected by well-defined continuous pathways of ED along which

the ED is a maximum relative to all neighboring paths. As the pathways resembled what were perceived as having the defining characteristic of bonded interactions, they mapped out all of the paths for several molecules and found that the atoms that were perceived to be bonded were connected by continuous pathways of maximum ED. The value of the ED along the paths between a pair of atoms was found to decrease from the nucleus of each pair to a local minimum value at a critical point (a saddle point) along the path where $\nabla\rho(\mathbf{r}) = 0$. The path of maximum ED connecting the nuclei of the pair was denoted the bond path and the point along the path where $\rho(\mathbf{r})$ is a local minimum was denoted the bond critical point, $\mathbf{r}_c$. It is the accumulation of the ED between the nuclei of the bonded atoms that is associated with the line of maximum ED (the bond path) connecting the nuclei. As the ED distribution adopted by a ground state system results in the lowest energy, a system with bond paths of maximum ED may be considered to be stabilized relative to one that lacks bond paths (Gatti 2005). As each bond path is also associated with a line of maximally negative potential energy density linking the pair, Bader (1998) concluded that the presence of a bond path together with its topologically equivalent virial path that also connects the pair serve as a universal indicator of a bonded interaction. Moreover, as the ED is topologically determined by the virial field, the presence of the virial path results in a line of maximum ED, a bond path and a state of electrostatic equilibrium between the pair. When these conditions are satisfied, the presence of a bond path linking a pair of atoms suffices as evidence that the pair is bonded. Indeed, all atomic interactions that result in bond paths, including those classified as nonbonded, are responsible for the binding of the atoms in molecules and crystalline materials (Bader 1998). In a study of bond path exchange-correlation energies, Pendas et al. (2007) recently presented evidence that bond paths represent direct electron exchange channels between a bonded pair that necessarily serve to stabilize not only the bonded interaction but also the system.

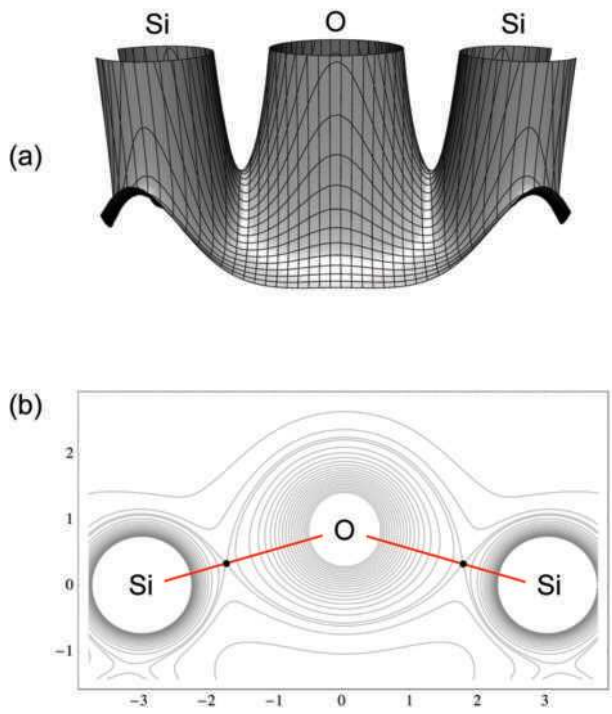

FIGURE 1. Electron density, ED, distribution for the $H_6Si_2O_7$ molecule, calculated at the B3LYP/6-311(2d,p) level through the bridging Si-O-Si angle of the molecule and plotted as a (**a**) level line relief ED map calculated between $\rho(r) = 0.0$ and 0.3 a.u. and (**b**) in a level line contour map calculated between $\rho(\mathbf{r}) = 0.0$ and 1.0 a.u. in intervals of 0.05 a.u. The level contour line in **b** that is connected by the black dots along the ridge between the Si and O atom was calculated at the 0.136 a.u. level, the value of $\rho(\mathbf{r}_c)$. The black dots show the locations of the Si-O bond critical points along the Si-O bridging bond paths. The peak heights of the Si and O atoms tower above the ED along the bond paths at heights of ~550 and ~160 a.u., respectively (1 a.u. = 6.748 e/Å^3).

BOND PATHS AND BRIDGING Si-O BONDED INTERACTIONS FOR THE $H_6Si_2O_7$ MOLECULE

The ED distribution associated with the Si-O-Si bridging angle for the $H_6Si_2O_7$ molecule is displayed in Figures 1a and 1b. Both maps were calculated in the plane of the Si-O-Si angle at the B3LYP/6-311(2d,p) level. Figure 1a displays a contoured level line relief map of the ED distribution for the molecule calculated between 0.0 and 0.3 a.u. (1 a.u. = 6.748 e/A^3), resulting in extremely large maxima centered on the bridging O and the two coordinating Si atoms of the angle. The two Si atoms are connected to the O atom by well-defined ridges of ED running between the nuclei of the atoms. As the ridges are due to the accumulation of the ED along the bond paths, their presence is consistent with the bonded interactions that exist between the Si and O atoms. The ridges decrease in height from the nuclei of the Si and O atoms to a local minimum value in the ED, $\rho(\mathbf{r}_c)$, between the contoured atoms at bond critical points. Figure 1b is a level line contour map of the same ED distribution between 0.0 and 1.0 a.u. with a contour interval of 0.05 a.u., with the exception of one contour that was drawn at the $\rho(\mathbf{r}_c) = 0.136$ a.u. level. Like the relief map, the contour map shows that the Si and O atoms are connected by well-defined ridges of ED that decrease in value along the bond paths toward $\mathbf{r}_c$ (denoted by black dots in Fig. 1b). Note that the contour line constructed at the $\rho(\mathbf{r}_c)$ level intersects at the local minima along the ridges between the Si and O atoms, locating the positions of the bond critical points for the two bridging Si-O bonded interactions. The separation between the Si and O atoms (the Si-O bond length) is directly related to the value of ED at $\mathbf{r}_c$; with few exceptions, the greater the value of $\rho(\mathbf{r}_c)$, the shorter the Si-O bond length and the greater the strength of the bonded interaction. Also, the distances between the nuclei and the bond critical points (measured along the two bond paths) define the bonded radii for the two atoms, denoted r_b(Si) and r_b(O), respectively (Bader 1990). The bonded interaction involving the Si and O atoms of the molecule is considered to be the result of the net electrostatic attraction imposed on the nuclei of the pair by the accumulation of ED along the bond path in the vicinity between the nuclei, balancing the forces of repulsion between the nuclei and stabilizing the structure (Feynman 1939). Furthermore, by counting all the bond paths that radiate from a given atom to adjacent atoms, an unambiguous determination of the coordination number of the atom can be made (Gibbs et al. 1992).

The Laplacian, $\nabla^2\rho(\mathbf{r})$, a tool for locating Lewis acid and base sites

A set of nested level surfaces (isosurfaces) of ED, calculated around a section of one of the Si-O bridging bond paths of the $H_6Si_2O_7$ molecule is displayed in Figure 2a. The isosurfaces show that the ED increases systematically in value in the direction of the bond path, adopting a saddle point, a maximum value adjacent to the bond path and a local minimum value at $\mathbf{r}_c$ along the path. The shape of the ED distribution in the immediate vicinity of the bond critical point is displayed more clearly in Figure 2b by a single isosurface with a $\rho(\mathbf{r})$ value of 0.1300 a.u., close to $\rho(\mathbf{r}_c)$ = 0.1360 a.u.. An examination of the isosurface shows that it represents a single-sheeted hyperboloidal distribution of ED around the bond path with three well-defined curvatures at its extrema (Marsden and Tromba 1976). Note that the ED is distributed cylindrically about the bond path reflecting the high σ character and the lack of π character of the bond. As a Taylor series is well suited for characterizing the extrema for such a well-behaved distribution, a Taylor series of second-order partial derivatives was used to model the topology of the ED distribution in the immediate vicinity of $\mathbf{r}_c$. With this strategy, the curvatures and the Laplacian of the ED at the bond critical point along a bond path can be determined with a Taylor series expansion of the ED about $\mathbf{r}_c$, as discussed by Bader (1990).

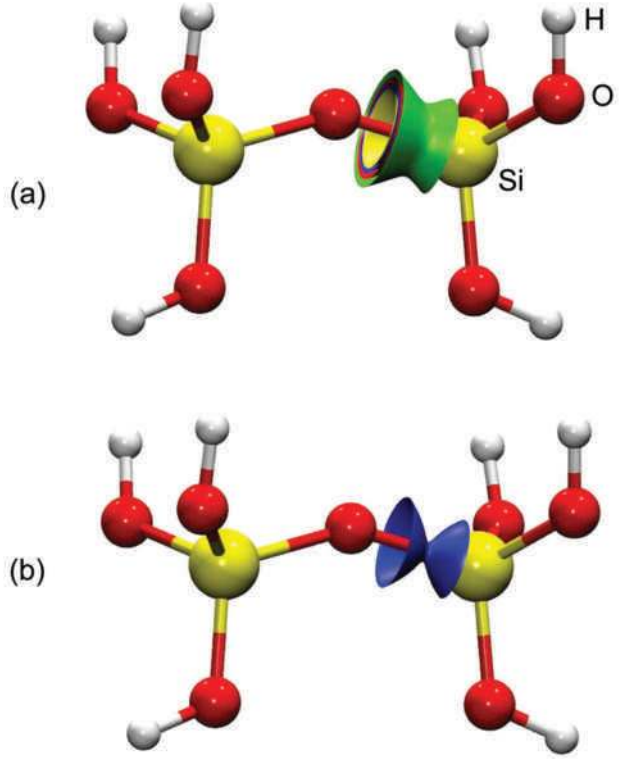

Figure 2. (**a**) A segment of a nested set of level isosurfaces of the ED distribution calculated at intervals of 0.0275 a.u. at the B3LYP/6-11(2d,p) level around one of the Si-O bridging bond paths of the $H_6Si_2O_7$ molecule. The outermost green level isosurface was calculated at the $\rho(\mathbf{r})$ = 0.0750 a.u. level, the next inner red one was calculated at the $\rho(\mathbf{r})$ = 0.1025 a.u. level, the blue one at the $\rho(\mathbf{r})$ = 0.1300 a.u. level, and the innermost yellow one was calculated at the $\rho(\mathbf{r})$ = 0.1575 a.u. level. (**b**) The same figure as **a** except all of the level isosurfaces have been deleted except the blue one that was calculated at the $\rho(\mathbf{r})$ = 0.13 level, a value close to that at the bond critical point, $\rho(\mathbf{r}_c)$ = 0.136 e/Å^3. The blue isosurface can be described as a single-sheeted hyperboloid around the Si-O bond path (see Fig. 2.1.13, Marsden and Tromba 1976). The red spheres of the molecule represent O atoms, the white ones H, and the yellow ones Si. The red and yellow rods connecting the Si and O atoms and the red and white ones connecting the O and H atoms represent the bond paths of the molecular graph of the molecule.

For a given bonded interaction, the components for the Taylor series can be determined by measuring the values of $\rho(\mathbf{r})$ at 27 points in the immediate vicinity of $\mathbf{r}_c$, at the corners, the centers of each of the edges and faces and the center of a tiny cube, ~10^{-6} a.u., on an edge, centered at $\mathbf{r}_c$ and fitted to the second-order Taylor series expansion:

$$\rho(\mathbf{r}) = \rho(\mathbf{r}_c) + (\mathbf{r} - \mathbf{r}_c)^t\nabla\rho(\mathbf{r}) + 1/2(\mathbf{r} - \mathbf{r}_c)^t H_{ij}(\mathbf{r} - \mathbf{r}_c)$$

where $\nabla\rho(\mathbf{r}_c) = 0$ and $H_{ij} = \partial^2\rho(\mathbf{r}_c)/\partial x_i\,\partial x_j$, i,j = (1,2,3). As H_{ij} is a real and symmetric Hessian matrix, it can be transformed into diagonal form, Λ, where the diagonal elements define the curvatures of $\rho(\mathbf{r}_c)$ along the associated eigenvectors $\mathbf{e}_i$, i = (1,2,3). The trace of Λ, $tr(\Lambda) = \lambda_1 + \lambda_2 + \lambda_3$ where $\lambda_1 = \partial^2\rho(\mathbf{r}_c)/\partial x_1^2$, $\lambda_2 = \partial^2\rho(\mathbf{r}_c)/\partial x_2^2$ and $\lambda_3 = \partial^2\rho(\mathbf{r}_c)/\partial x_3^2$ is the Laplacian $\nabla^2\rho(\mathbf{r}_c)$ of $\rho(\mathbf{r}_c)$. As observed above, the signs of two principal components λ_1 and λ_2 are both negative while λ_3 is positive. Collectively, $\rho(\mathbf{r}_c)$, the three curvatures λ_1 , λ_2, and λ_3 of $\rho(\mathbf{r}_c)$ and $\nabla^2\rho(\mathbf{r}_c)$ are referred to as the bond critical point, bcp, properties of a bonded interaction (Bader 1990).

In general, the value of the Laplacian of the ED, $\nabla^2\rho(\mathbf{r})$, measures the extent to which the ED is either locally concentrated or depleted at a given point $\mathbf{r}$ in the distribution (Bader and Essén 1984). If $\nabla^2\rho(\mathbf{r})$ is positive, then the value of $\rho(\mathbf{r})$ is less than all surrounding points lying on the surface of a sphere of radius d$\mathbf{r}$ centered at $\mathbf{r}$, and the ED is said to be locally depleted at $\mathbf{r}$. On the other hand, when $\nabla^2\rho(\mathbf{r})$ is negative, the converse is true and the ED is said to be locally concentrated at $\mathbf{r}$ (Lieb and Loss 1997). To appreciate the topology of the ED distribution for an

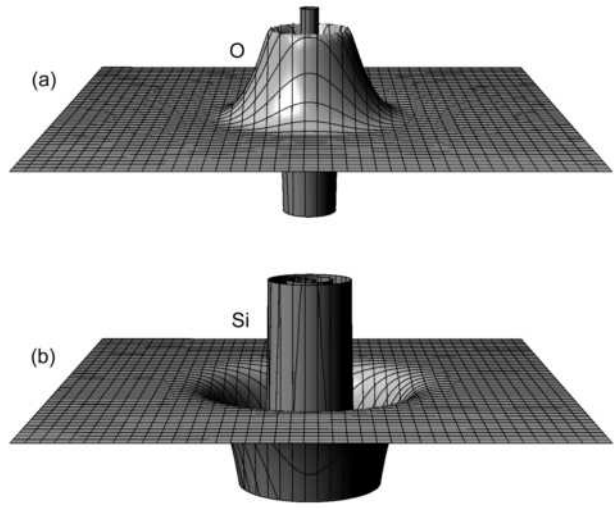

Figure 3. $L(\mathbf{r}) = -\nabla^2\rho(\mathbf{r})$ (a.u.) level line relief maps calculated at the B3LYP/6-311(2d,p) level in a plane containing the nucleus for an isolated (**a**) O atom with the contribution of one core orbital neglected and (**b**) an isolated Si atom. The maps were cut off at the ±15 a.u. level (1 a.u. = 24.099 e/Å^5).

isolated O atom in terms of the Laplacian (Fig. 3a), an $L(\mathbf{r}) = -\nabla^2\rho(\mathbf{r})$ level line relief map was calculated for the atom at the B3LYP/6-311(2d,p) level in a plane passing through its nucleus with the contribution of one core orbital neglected [note that $L(\mathbf{r})$ is positive in regions where the ED is locally concentrated and negative in regions where it is locally depleted]. The map displays two sets of spherical nodes each centered on the nucleus, representing the shell structure of the atom. For each principle quantum shell of the atom, there is a pair of concentric regions, one positive and one negative. The positive ones define spherical regions of locally concentrated ED and the negative ones define concentric spherical regions of locally depleted ED. Together, the two sets of locally concentrated and locally depleted regions of ED correspond to the *K* and *L* quantum shells of the O atom (Bader et al. 1984). The outermost shell of locally concentrated ED defines the chemically important valence shell charge concentration, VSCC, of the O atom. The VSCC is at a distance of 0.66 Å from the nucleus, comparable to both the atomic radius, 0.65 Å (Bragg 1920) and the maximum in the radial charge density of the shell, 0.60 Å, of the O atom (Slater 1964). Upon forming a bonded interaction with Si, for example, the VSCC of the atom is distorted to one degree or another and typically maxima are formed in the bonded and nonbonded domains. Despite the shell structure of an atom, it is noteworthy that, throughout space, the ED distribution decays monotonically away from the nucleus along a radial line in all directions. An $L(\mathbf{r})$ level line relief map, calculated for an isolated Si atom at the B3LYP/6-311(2d,p) level (Fig. 3b), displays a spike-like *K* shell at its center enclosed by a well-developed *L* shell that in turn is enclosed by a very diffuse low-lying VSCC *M* shell. As the VSCC for the Si atom is diffuse and very low-lying and situated substantially further from the nucleus than that of the O atom, it fails to show well-defined distortion features in its valence shell upon chemical combination with O (Bader 1990).

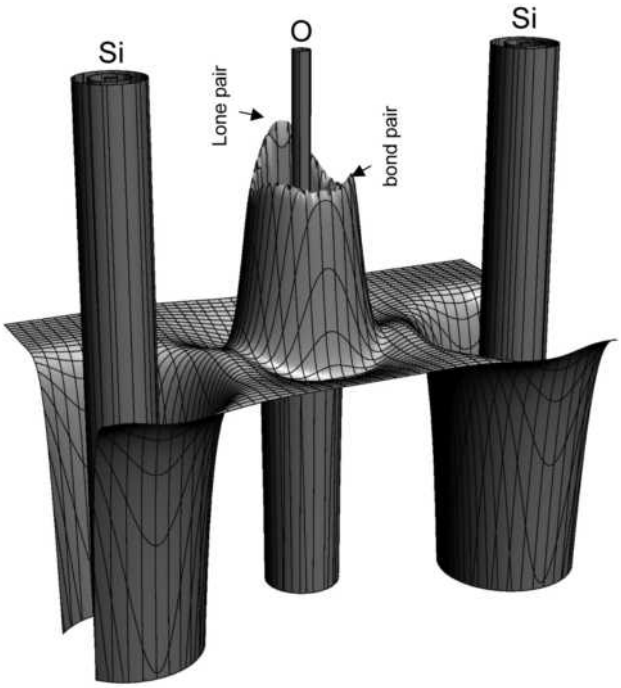

FIGURE 4. $L(\mathbf{r})$ level line relief map for the $H_6Si_2O_7$ molecule calculated at the B3LYP/6-311(2d,p) level in the plane containing the Si-O-Si angle with contributions from all of the core orbitals included. The bridging O is located at the center of the figure and the two Si are located at the edges of the figure. The map was cut off at ±5 a.u. level.

In a determination of the extent to which the VSCC for the bridging O atom of the Si-O-Si angle is distorted with the formation of the $H_6Si_2O_7$ siloxane molecule, $L(\mathbf{r})$ was mapped in the plane of the angle (Fig. 4). As for the Si and O atoms, the $L(\mathbf{r})$ relief map for the molecule was calculated at the B3LYP/6-311-(2d,p) level, but unlike the calculations for the O atom, all the core orbitals were included. The features surrounding the two Si atoms in Figure 4 are very similar to those displayed in the immediate vicinity of the isolated atom (Fig. 3b). In contrast, the VSCC for the O atom is distorted substantially, with the formation of one well-defined maximum located on the reflex side of the Si-O-Si angle with a low-lying narrow ring of locally concentrated ED extending into the interior of the angle with two very low-lying maxima located where the two Si-O bond paths cross the ring (Gibbs et al. 1994). The small maxima are associated with the local concentration of ED along the Si-O bond paths and their interaction with the VSCC of the O atom. The larger maximum represents a region of locally concentrated ED in the nonbonded region of the O atom on the reflex side of the Si-O-Si angle, while the two low-lying maxima on the interior of the angle represent the local concentration of the ED in the Si-O bonding domain. The Si-O bonding domain is defined by the polarization of the concentrated ED associated with the O atom toward the Si atom reported in an earlier study of the molecule (Gibbs et al. 2004) and that reported for the bridging O2 O atom in beryl, $Al_2(Be_3Si_6O_{18})$ (Prencipe et al. 2002), a feature that indicates that the Si-O bond has a component of shared character (Bader and Essén 1984). This feature and its bearing on the character of a Si-O bonded interaction will be discussed in more detail below.

As is typical, the nonbonded maxima displayed in Figure 4 are substantially larger in magnitude than bonded ones (Bader 1990). It is noteworthy that in regions where $L(\mathbf{r})$ is positive, the ED is more tightly bound and compressed (concentrated) above its average distribution such that the potential energy dominates the kinetic energy of the local ED. Given the substantially larger maximum in the nonbonded region of the O atom, compared with the diffuse ring and lower maxima in the bonded region, the potential energy of the electrons in the lone pair region is indicated to be greater than that in the binding region, indicating that the electrons in the lone pair region serve to stabilize the Si-O-Si bonded interactions to a greater extent than those in the bond pair region.

As it is relatively difficult to infer from a relief map the spatial features associated with the maxima, a three-dimensional $L(\mathbf{r})$ isosurface map was generated in the immediate vicinity of the bridging O atom of the $H_6Si_2O_7$ molecule (Fig. 5a). The map shows that the atom is capped by a bracelet-shaped isosurface of locally concentrated ED with its maximum (a Lewis base domain) located on the reflex side of the Si-O-Si angle. Isosurface maps were calculated in an earlier experimental study for the five nonequivalent O atoms for the high-pressure silica polymorph, coesite (Gibbs et al. 2003b). Like the map for the $H_6Si_2O_7$ molecule, it is noteworthy that the maps displayed little

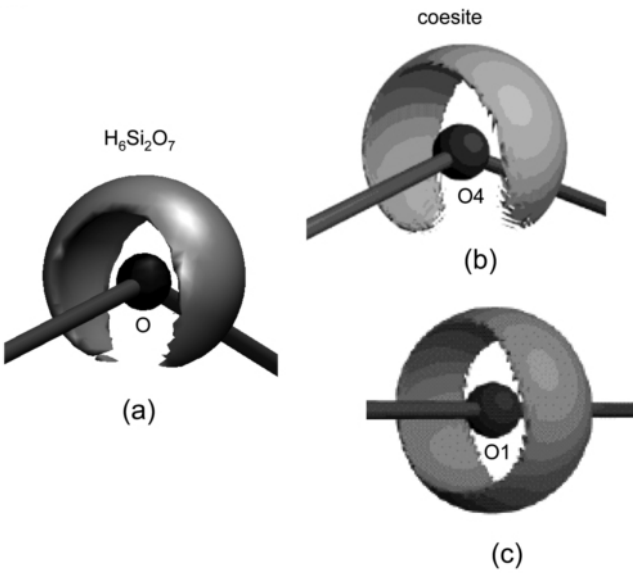

FIGURE 5. $L(\mathbf{r})$ level line isosurface maps generated for the nonbonded domains for the bridging O atoms for (**a**) the $H_6Si_2O_7$ molecule and for the (**b**) O4 and the (**c**) O1 oxygen atoms of coesite, respectively (Gibbs et al. 2003b), each constructed in the immediate vicinity of the plane that bisects the Si-O-Si angle. The Si-O-Si angles involving the bridging O of the molecule and the O4 atom of coesite are both ~144°, whereas O1 is involved in a 180.0° angle. The maxima of the bracelet-shaped isosurfaces are located on the reflex side of the angle, while the maxima encircle the O1 atom in a continuous ring. The dark gray spheres at the center of each figure represent O atoms and the rods radiating from the spheres represent segments of the Si-O bond paths.

or no features in the bonded regions along the Si-O bonds. Also, like the O atom of the molecule, four (O2, O3, O4, and O5) of the five nonequivalent O atoms in coesite display bracelet-shaped isosurfaces capping the atoms with their maxima also located on the reflex side of the Si-O-Si angles. The map generated for O4 is strikingly similar to those calculated for O2, O3, and O5 (not shown here; see Gibbs et al. 2003b, column 1, Fig. 5) and the bridging O atom of the $H_6Si_2O_7$ molecule, evidence that the properties of the ED for O atoms in coesite and in $H_6Si_2O_7$ are comparable. The map calculated for the molecule (Fig. 5a) is compared with those calculated for the O4 and O1 atoms in coesite in Figures 5b and 5c, respectively (the O4 atom and the O atom in the molecule are both involved in Si-O-Si angles of ~145°, whereas O1 is involved in an 180° angle). In contrast, the isosurface calculated for O1 is a ring-torus shaped feature that encircles the atom unlike the bracelet-shaped isosufaces that cap the remaining O atoms in the coesite structure and in the $H_6Si_2O_7$ molecule. With the Si-O-Si angle for the $H_6Si_2O_7$ molecule clamped at 180.0°, a $L(\mathbf{r})$ level line map generated for the bridging O also displays ring-torus isosurface like that displayed about the O1 atom in coesite (Gibbs et al. 2003a). A similar torus-shaped feature has also been reported to exist on the O atom of the wide 170.2° Si-O-Si bonded interaction for beryl (Prencipe and Nestola 2007).

In a survey of the bonded and nonbonded domains and reactivity for several molecules, Bader et al. (1984) observed that regions of maximum local concentration of the ED in the VSCC of an atom correspond with Lewis base domains (sites of potential electrophilic attack by H, for example), whereas regions of maximum depletion in the VSCC correspond with Lewis acid sites. With this connection, the incorporation of H in the coesite structure at high temperatures and pressures via the hydrogarnet substitution mechanism (Koch-Muller et al. 2001) can be understood in terms of the electrophilic attack by the H atom at the nonbonded bracelet-shaped Lewis base domains of the four O atoms involved in the bent Si-O-Si angles of the structure with the concomitant loss of the Si atom from the structure (Gibbs et al. 2003b). The O1 atom is not involved in the substitution mechanism for the following reasons: it is involved in a straight (180°) angle, it is involved in an adjacent nonequivalent silicate SiO_4 unit, and it displays a ring-torus shaped isosurface with a maximum value along the ring less than that observed for the other O atoms in the structure [the calculated maxima for the five O atoms increase linearly with decreasing Si-O-Si angle as follows (1.0 a.u. = 24.099 e/Å^5): O1, 7.59 a.u., <Si-O-Si = 180°; O4, 7.84 a.u., <Si-O-Si = 149.7°; O3, 7.93 a.u., <Si-O-Si = 144.2°; O2, 7.93 a.u., <Si-O-Si = 142.0°; O5, 7.97 a.u., <Si-O-Si = 136.7°]. The progressive increase in the magnitude of the maxima with the narrowing of the angle indicates that an O atom becomes progressively more basic in character and more susceptible to attack by H as the Si-O-Si angle narrows. A similar result was reported in a study of the electron localization function, ELF, where the maxima in the ELF isosurface maps of the nonbonded regions of the bridging O of the Si-O-Si angles for coesite and several siloxane molecules also increase with decreasing angle (Gibbs et al. 2003b, 2005a). This result provides additional evidence for the assertion that the bonded interactions in a siloxane molecule are virtually the same as those for a silica polymorph (Gibbs et al. 2003b). In short, the O atoms involved in the hydrogarnet substitution involve the bent Si-O-Si angles and possess bracelet-shaped $L(\mathbf{r})$ isosurfaces with maxima that increase in magnitude with decreasing angle. In contrast, on the basis of an ad hoc electrostatic site potential model that assumes that coesite is fully ionic, Smyth (2006) concluded that of the five nonequivalent O atoms in coesite, only O1 is the most likely to be protonated, contrary to the earlier findings of the Koch-Muller et al. (2001) infrared study. Last, with the progressive localization of the ED in the lone pair regions [the nonbinding regions (Berlin 1951; Spackman and Maslen 1985)] of the bridging O atoms of coesite, the observed increase in the experimental Si-O bond lengths with decreasing Si-O-Si angle reported by Gibbs et al. (1977) is expected, without the need to resort to (Si_{3d}-O_{2p}) π arguments to explain the weakening of the bonds and the concomitant correlation between the bond length and the angle, the narrower the angle, the greater the concentration of the ED density in the nonbinding region, and the weaker and longer the Si-O bond (Gibbs et al. 1994).

Si-O BOND CRITICAL POINT PROPERTIES

In an earlier study of the ED distributions associated with the Si-O bonded interactions for a relatively large number of silicates, the bond critical point properties were calculated (Gibbs et al. 2001) and compared with model experimental properties (Gibbs et al. 2008a). The calculated properties are plotted in Figure 6 with respect to the experimental Si-O bond lengths, R(Si-O). With the accumulation of the ED at the bond critical points, the

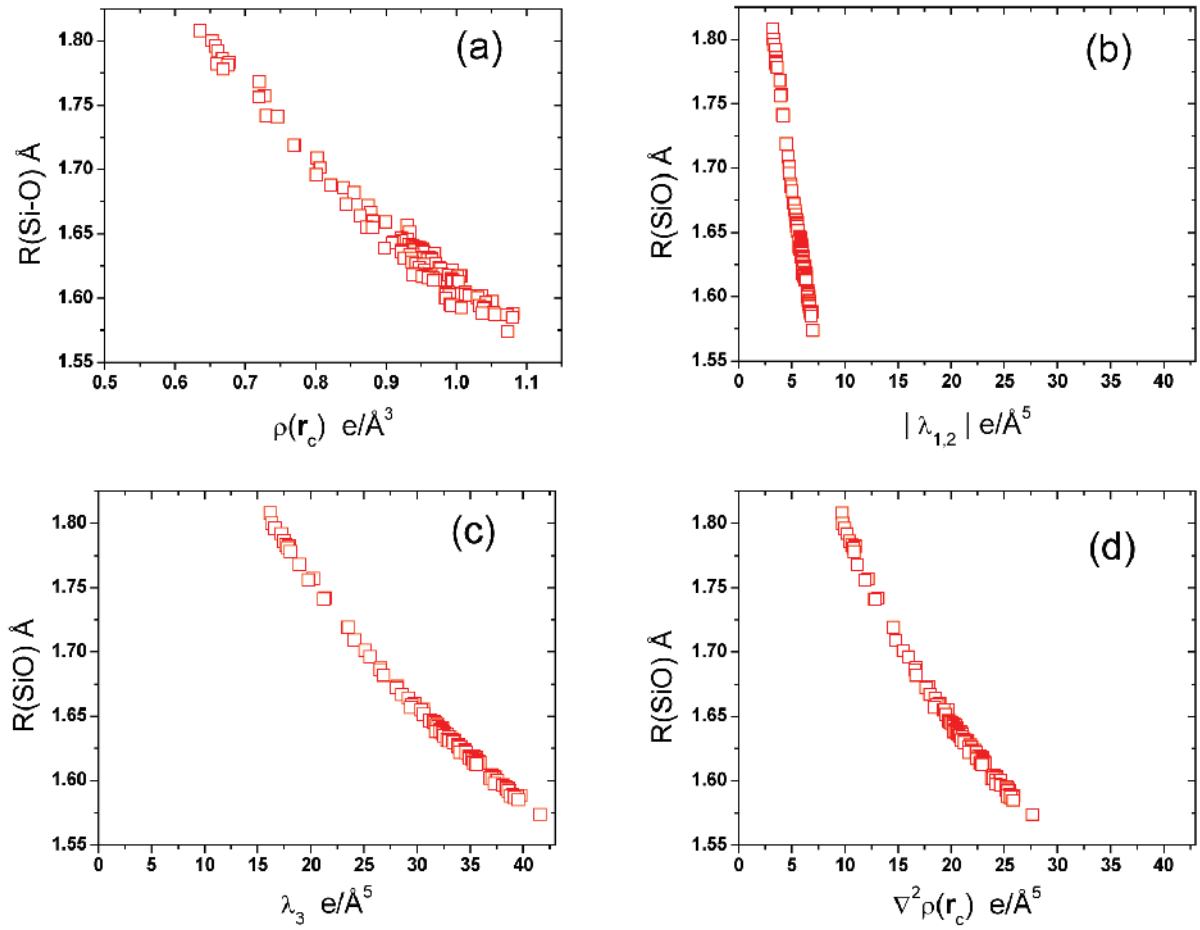

FIGURE 6. Calculated bond critical point properties for the Si-O bonded interactions for the experimental structures determined for several silicates and model structures for geometry optimized siloxane molecules (Gibbs et al. 2001), plotted with respect to their experimental Si-O bond lengths, R(Si-O) Å. (**a**) $\rho(\mathbf{r}_c)$ e/Å^3, the value of the electron density at the bond critical point, $\mathbf{r}_c$, plotted with respect to R(Si-O), (**b**) $|\lambda_{1,2}| = |\frac{1}{2}(\lambda_1 + \lambda_2)|$ e/Å^5 plotted with respect to R(Si-O), where λ_1 and λ_2 measure the local concentration of $\rho(\mathbf{r}_c)$ perpendicular to the bond path, (**c**) λ_3 e/Å^5, plotted with respect to R(Si-O), where λ_3 measures the local concentration of $\rho(\mathbf{r}_c)$ parallel to the bond path in the directions of the Si and O atoms (**d**) $\nabla^2\rho(\mathbf{r}_c)$ e/Å^5, the Laplacian of the electron density at $\mathbf{r}_c$, plotted with respect to R(Si-O).

Si-O bond lengths generally decrease, with a few exceptions, in a roughly linear trend (Fig. 6a). At $\mathbf{r}_c$, the curvatures, λ_1 and λ_2, of the ED, are both negative and decrease in value linearly as R(Si-O) decreases. As λ_1 and λ_2 measure the extent to which the ED is locally concentrated perpendicular to the bond path, the systematic decrease of the two curvatures with decreasing bond length indicates that the ED becomes progressively more locally concentrated toward the bond path at $\mathbf{r}_c$ as the bond length decreases. As $\lambda_1 \sim \lambda_2$ for the bulk of the bonded interactions in the silicates, we may conclude that the distributions of the ED in cross sections of the bond paths passing through $\mathbf{r}_c$ are generally circular, a result that indicates that the Si-O bonded interactions are relatively stable and are primarily σ-type bonded interactions with little or no π character (Bader et al. 1983). The average magnitude of the two, $|\lambda_{1,2}| = \frac{1}{2}(|\lambda_1 + \lambda_2|)$, is plotted in Figure 6b with respect to R(Si-O) where $|\lambda_{1,2}|$ increases slightly with decreasing bond length. The value of the third curvature, λ_3, measures the extent to which the ED is locally concentrated along the bond path at $\mathbf{r}_c$; the larger the value of λ_3, the greater the local concentration of the ED into the basins of the two atoms (Bader 1985; see below) and the greater the shielding of the nuclei. Figure 6c shows that the value of λ_3 increases substantially more, relative to $|\lambda_{1,2}|$, with decreasing bond length, indicating that the decrease in Si-O bond length is related in part to the extent to which nuclei of the Si and O atoms are progressively shielded with decreasing bond length. As the value of λ_3 is substantially larger than that of either λ_1 or λ_2, the sign of $\nabla^2\rho(\mathbf{r}_c)$ is necessarily positive. Also, inasmuch as the value of λ_3 increases at a faster rate than λ_1 and λ_2 both decrease, $\nabla^2\rho(\mathbf{r}_c)$ increases substantially as the bond length decreases and $\rho(\mathbf{r}_c)$ increases. As $1/4\nabla^2\rho(\mathbf{r}_c) = 2G(\mathbf{r}_c) + V(\mathbf{r}_c)$ increases, the negative definite local potential energy, $V(\mathbf{r}_c)$, decreases and the positive definite local kinetic energy, $G(\mathbf{r}_c)$, increases, with $V(\mathbf{r}_c)$ decreasing at a faster rate than $G(\mathbf{r}_c)$ increases such that the total local energy density, $H(\mathbf{r}_c) = G(\mathbf{r}_c) + V(\mathbf{r}_c)$, is negative and decreases as R(Si-O) decreases and $\rho(\mathbf{r}_c)$ increases at the bond critical point of the bonded interaction. For first and second row metal atoms (Li to B and Na to S) bonded to O, $\nabla^2\rho(\mathbf{r}_c)$ is positive in value and increases linearly with the value of $\rho(\mathbf{r}_c)$ as the bond lengths decrease (Gibbs et al. 2006b). Concomitant with these changes, the total energy density is positive for the bonded interactions involving the more electropositive atoms (Li, Na, and Mg), whereas it is negative

for the remaining more electronegative atoms, with the value of $H(\mathbf{r}_c)$ becoming progressively more negative as the bond length decreases and $\nabla^2\rho(\mathbf{r}_c)$ increases in value. In contrast, the $H(\mathbf{r}_c)$ values for the bonded interactions involving the Li, Na, and Mg atoms become progressively more positive with decreasing bond length and the increasing value of $\rho(\mathbf{r}_c)$.

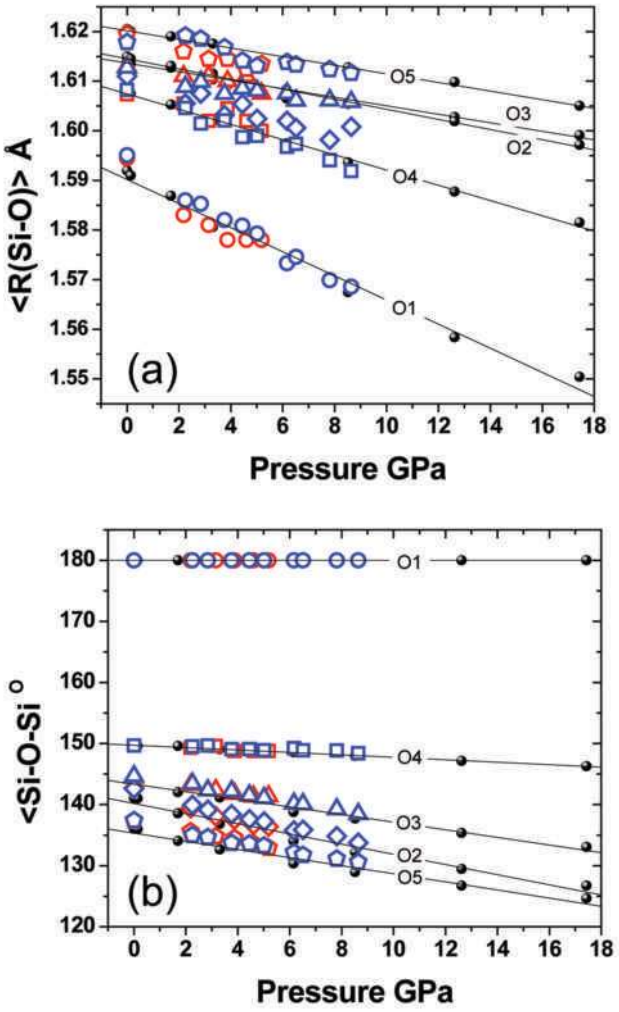

FIGURE 7. (**a**) A comparison of <R(Si-O)>, the average of the two Si-O bond lengths comprising each of the nonequivalent Si-O-Si angles and (**b**) the five nonequivalent Si-O-Si angles for coesite plotted with respect to pressure. The black dots represent data obtained by optimizing the coesite structure as a function of pressure, red symbols represent experimental data determined by Levien and Prewitt (1981), and the blue ones represent experimental data determined by Angel et al. (2003). The red and blue circles represent Si-O1 bonded interactions, the red and blue diamonds represent Si-O2 bonded interactions, red and blue triangles represent Si-O3 bonded interactions, red and blue squares represent Si-O4 bonded interactions, and red and blue pentagons represent Si-O5 bonded interactions. (**b**) A comparison of the Si-O-Si angles calculated for coesite plotted with respect to pressure (black dots). The experimental Si-O-Si angles are plotted in the figure as red and blue symbols. The data plotted as red symbols were determined by Levien and Prewitt (1981), and the ones plotted as blue symbols were determined by Angel et al. (2003). Solid lines were arbitrarily drawn through the calculated data (black dots) for coesite.

OPTIMIZED STRUCTURES AND EXPERIMENTAL ELECTRON DENSITY DISTRIBUTIONS

Using a classical Born 3-body potential model with Si^{4+} and O^{-2} ions and ad hoc pair bond bending terms, Sanders et al. (1984) found that the model was capable of generating accurate elastic constants and Si-O-Si angles measured at pressure for quartz and for several other polymorphs with silicate tetrahedral oxyanions. The model also generated dispersion curves that match the experimental curves within a few percent, a testament to their careful crafting of the model. Several hypothetical silica structures (Boisen and Gibbs 1993) were subsequently examined with non-classical first-principles total energy pseudopotential methods and the structural parameters, cohesive energies and bulk moduli were found to be comparable with those observed for low quartz, low cristobalite, and silica sodalite (Teter et al. 1995). In addition, experimental molar volume-pressure trends were reproduced for quartz, cristobalite, and stishovite together with their bulk moduli. The crystal structures of quartz, coesite, and cristobalite have since been geometry optimized with first-principles methods for a range of pressures between 0.0 and ~17.0 GPa (Demuth et al. 1999; Gibbs et al. 2000, 1999, 2008a). The optimized structures agree with those determined experimentally (Levien and Prewitt 1981; Levien et al. 1980; Angel et al. 2003; Downs and Palmer 1994) largely within the experimental error. Each of the model structures was generated by minimizing the total energy with respect to the unit-cell dimensions and the internal coordinates of the Si and O atoms for a prescribed set of unit-cell volumes, using density functional theory. The geometry optimized Si-O bond lengths and Si-O-Si angles obtained for coesite (Gibbs et al. 2000) are compared with the experimental bond values determined as a function of pressure (Levien and Prewitt 1981; Angel et al. 2003) in Figure 7. The bond lengths and angles are comparable, agreeing with the bulk of experimental data within ~1%. The bond lengths and angles optimized for quartz (Gibbs et al. 2008a), cristobalite (Downs and Palmer 1994), and the framework silicate beryl (Prencipe and Nestola 2007) show a similar agreement with the experimental values. The bcp properties calculated for the structures are virtually the same as those displayed in Figure 6, with the values falling within and along the scatter of the silicate data, the properties increasing slightly in value with decreasing bond length and increasing confining pressure. It is noteworthy that the ED distributions for the geometry optimized coesite and quartz structures change relatively little with compression (Gibbs et al. 2000, 1999) with the values of $\rho(\mathbf{r}_c)$ and $\nabla^2\rho(\mathbf{r}_c)$ increasing ~5 and ~10%, respectively, and $r_b(O)$ decreasing slightly (~2%), suggesting a small increase in the shared character of the Si-O bond. In the case of beryl, modeled over a larger range of pressures between ~0.0 and 28.4 GPa, $r_b(O)$ decreases ~5%, $\rho(\mathbf{r}_c)$ increases ~15%, and $\nabla^2\rho(\mathbf{r}_c)$ increases ~25%, indicating an increase in the shared character of the Si-O bonded interaction with increasing pressure (Prencipe and Nestola 2007). Despite the strong polarization of the local concentration of the ED associated with the O atom toward the bond pair region of the Si atoms and the formation of maxima in the bond pair region of beryl, Prencipe et al. (2002) considers it more appropriate to picture the Si-O bonded interactions in beryl as closed-shell ionic interactions by dint of their large positive $\nabla^2\rho(\mathbf{r}_c)$ values (~25 e/A^5) and the conformity of the bcp

properties with the criteria expected for a closed-shell bonded interaction (Bader and Essén 1984). Furthermore, as the value of $\nabla^2\rho(\mathbf{r}_c)$ increases substantially with increasing pressure, it was asserted later that the closed-shell character of the bonded interaction increases with pressure, despite the concomitant increase in the value of $\rho(\mathbf{r}_c)$ and the decrease in the bonded radii of the O atoms associated with the interaction (Prencipe and Nestola 2007). Yet, as will be discussed below, the increase in $\nabla^2\rho(\mathbf{r}_c)$ with increasing pressure may, in fact, indicate an increase in the shared character of the Si-O bonded interaction rather than an increase in the closed-shell character.

In addition to the experimental structural data obtained for quartz and coesite, experimental model ED distributions have been determined for the high-pressure silica polymorphs stishovite with $^{VI}SiO_6$ units (Kirfel et al. 2001) and coesite with $^{IV}SiO_4$ units (Gibbs et al. 2003b). The distribution for stishovite was determined with a single-crystal synchrotron X-ray diffraction data set, whereas that for coesite was determined with a single-crystal high-resolution X-ray diffraction data set. As experimental ED distributions necessarily contain relatively large diffraction ripples and other defects owing to incomplete data sets and systematic errors, the ED distributions were modeled with the multipolar formalisms of Stewart (1976). In the modeling strategy, the ED distribution associated with each nonequivalent atom in the crystal was represented by a spherical core and an aspherical valence shell of ED, the latter being unconstrained so that it could either expand or contract, depending on the atomic charge and the deformation of the valence shell ED distribution. Simply stated, the spherical core and the deformed valence ED distribution for each nonequivalent atom, i, was modeled with a spherical core, c, monopole, P_{ic}, and a multipole expansion, $P_{ilm}R_l(\mathbf{r})Y_{lm}(\theta,\phi)$, respectively, where P_{ic} and P_{ilm} are population

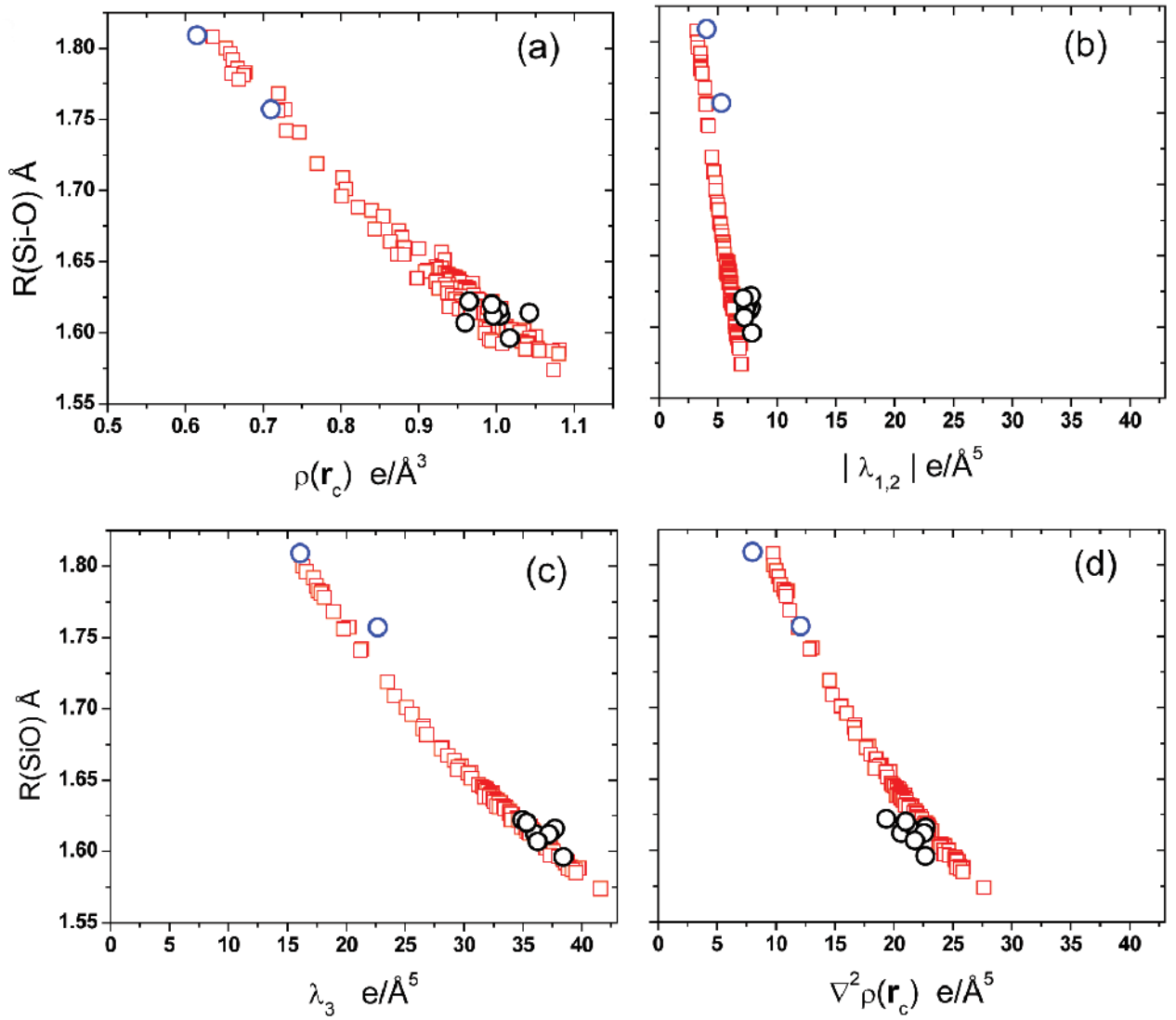

FIGURE 8. The experimental Si-O bond lengths, R(Si-O), for the silicates displayed in Figure 6, plotted with respect to (**a**) $\rho(\mathbf{r}_c)$, (**b**) $|\lambda_{1,2}|$, (**c**) λ_3, and (**d**) $\nabla^2\rho(\mathbf{r}_c)$, all plotted as red squares. Superimposed upon the calculated data are model experimental bond critical point properties determined for stishovite with high-resolution single-crystal synchrotron diffraction data by Kirfel et al. (2001) plotted as blue circles, and model properties determined for coesite high-resolution single-crystal data by Gibbs et al. (2003b) plotted as black circles.

parameters for the core and valence electrons, $R_i(\mathbf{r})$ is a radial distribution Slater type function or a linear combination of exponentials, and $Y_{lm}(\theta,\phi)$ is a suitable set of spherical tesseral harmonics (for a more complete treatment of the aspherical atom modeling strategy of the ED distribution, see Hansen and Coppens 1978).

The modeling of the aspherical ED distributions for the two silica polymorphs was undertaken with the elegant software VALRAY (Stewart et al. 2000), which applied the nucleus centered, flexible pseudoatom multipole expansion of the ED to each of the nonequivalent atoms. The experimental population parameters P_{ic} and P_{ilm} were determined in a least-squares refinement in terms of the observed structural amplitudes. Upon completion of the multipole refinement, the resulting model multipole representation of the ED distribution was subjected to a topological analysis in the determination of the experimental model bcp properties for the Si-O bonded interactions for stishovite and coesite.

The model experimental bcp properties for stishovite and coesite are compared in Figure 8 with the properties calculated for the silicates used to prepare Figure 6. The experimental properties for the two polymorphs follow the trends, for the most part, established by the calculated data with the experimental $\rho(\mathbf{r}_c)$, λ_3, $|\lambda_{1,2}|$, and $\nabla^2\rho(\mathbf{r}_c)$ values each increasing with the decreasing bond length. The experimental $\rho(\mathbf{r}_c)$ values for both polymorphs fall along and largely within the scatter of the calculated data, whereas the $|\lambda_{1,2}|$ values are somewhat larger than the calculated values. The λ_3 values fall within the scatter of the calculated values for the most part, whereas the $\nabla^2\rho(\mathbf{r}_c)$ values follow the trend of the calculated data but several of the coesite values depart slightly from the trend. Model experimental $\rho(\mathbf{r}_c)$ and $\nabla^2\rho(\mathbf{r}_c)$ properties determined for the Si-O bonded interactions in several olivines (Gibbs et al. 2008c), diopside (Bianchi et al. 2005), and scolecite (Kuntzinger et al. 1998) with synchrotron and high-resolution single-crystal data are comparable with the calculated values with the bulk of the experimental values agreeing, for the most part, within ~10%. In addition, model experimental bcp properties for the Mg-O, Fe-O, Mn-O, and Co-O bonded interactions, determined with single-crystal synchrotron X-ray diffraction data sets for the olivines, are also comparable with calculated values (Gibbs et al. 2008b). It is noteworthy that the experimental model bcp properties determined for Fe-O, Mn-O, and Co-O bearing organometallic polymers scatter along the experimental and calculated trends observed for the olivines Fe_2SiO_4, Mn_2SiO_4, and Co_2SiO_4 (Gibbs et al. 2008b).

As a point of interest, the model experimental $\rho(\mathbf{r}_c)$ values generated for coesite and stishovite correlate with the Brown and Shannon empirical bond strengths for the interactions (Gibbs et al. 2004). Based on correlations established between bond length and bond number, Brown and Shannon (1973) found that the Si-O bond lengths for a large number of silicates could be connected to the empirical bond strengths, s, of the bonds with the power law expression $s = [(R(\text{Si-O})/1.625]^{4.5}$. Using this expression, the empirical bond strengths were calculated for the bulk of the Si-O bonds used to construct Figure 6 and plotted with respect to the $\rho(\mathbf{r}_c)$ values calculated for the silicates (Gibbs et al. 2004) (Fig. 9). As the bond strength increases, the value of $\rho(\mathbf{r}_c)$ increases in tandem in a regular way. The s values, calculated with the experimental bond lengths for coesite and stishovite, are plotted in Figure 9 with respect to the experimental $\rho(\mathbf{r}_c)$ values determined for the silica polymorphs. Despite the empirical connection between bond strength and bond length, the agreement between the bond strength and the ED values for coesite and stishovite is a testament to Pauling's (1929) definition and the Brown and Shannon (1973) modeling of the electrostatic bond strength. The comparability of the empirical bond strength and $\rho(\mathbf{r}_c)$ is also a testament to Pauling's genius in his definition of his second rule.

Siloxane molecules and silicates

In addition to the properties calculated for the bonded interactions for silicates, bcp properties have also been calculated for several geometry optimized siloxane molecules (Gibbs et al. 1998). The Si-O bond lengths for the molecules range between 1.515 Å for a ^{III}Si-O bonded interaction, 1.624 Å for a ^{IV}Si-O bonded interaction, 1.742 Å for a ^{VI}Si-O bonded interaction, and 2.009 Å for a ^{VIII}Si-O bonded interaction. As the optimized Si-O bond lengths decrease, the values of $\rho(\mathbf{r}_c)$, $|\lambda_{1,2}|$, λ^3, and $\nabla^2\rho(\mathbf{r}_c)$ each increase as observed for the silicates (Fig. 10). In each case, the bulk of the molecular data fall within and scatter along the trends established for the silicates when plotted with respect to the geometry optimized bond lengths (Gibbs et al. 2006a). The agreement between the two data sets shows that the properties of the ED in the vicinity of the bond critical point for the siloxane molecules and the silicate crystals are comparable, a result that is consistent with the close similarity of the bond lengths and angles exhibited by the silica polymorphs and siloxane molecules (Gibbs 1982). The agreement in properties extends to the mean enthalpy for the bridging Si-O bonds for quartz (465 kJ/mol), which is virtually the same as that calculated for the $H_6Si_2O_7$ molecule (462 kJ/mol) (O'Keeffe, personal communication). The close agreement of the enthalpies together with the ED distributions displayed by the $H_6Si_2O_7$ molecule and coesite, and the comparability of the Si-O bond critical point proper-

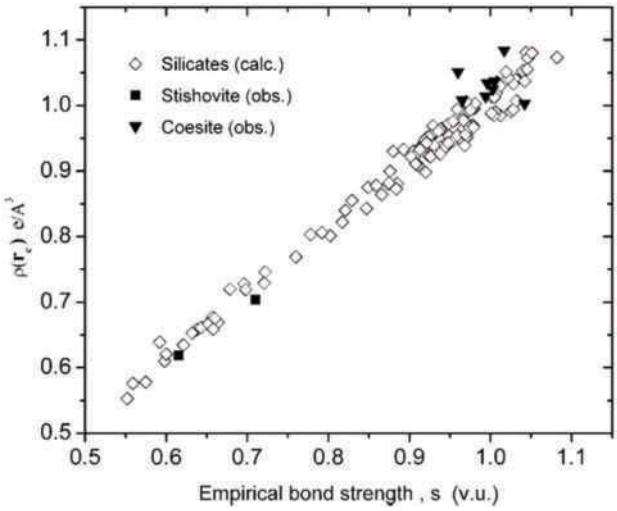

Figure 9. The $\rho(\mathbf{r}_c)$ values calculated for silicate crystals (diamonds) and the model experimental $\rho(\mathbf{r}_c)$ values determined for coesite (solid triangles) and stishovite (solid squares), plotted with respect to the Brown and Shannon (1973) empirical bond strength, s, calculated with the experimental Si-O bond lengths (Gibbs et al. 2004).

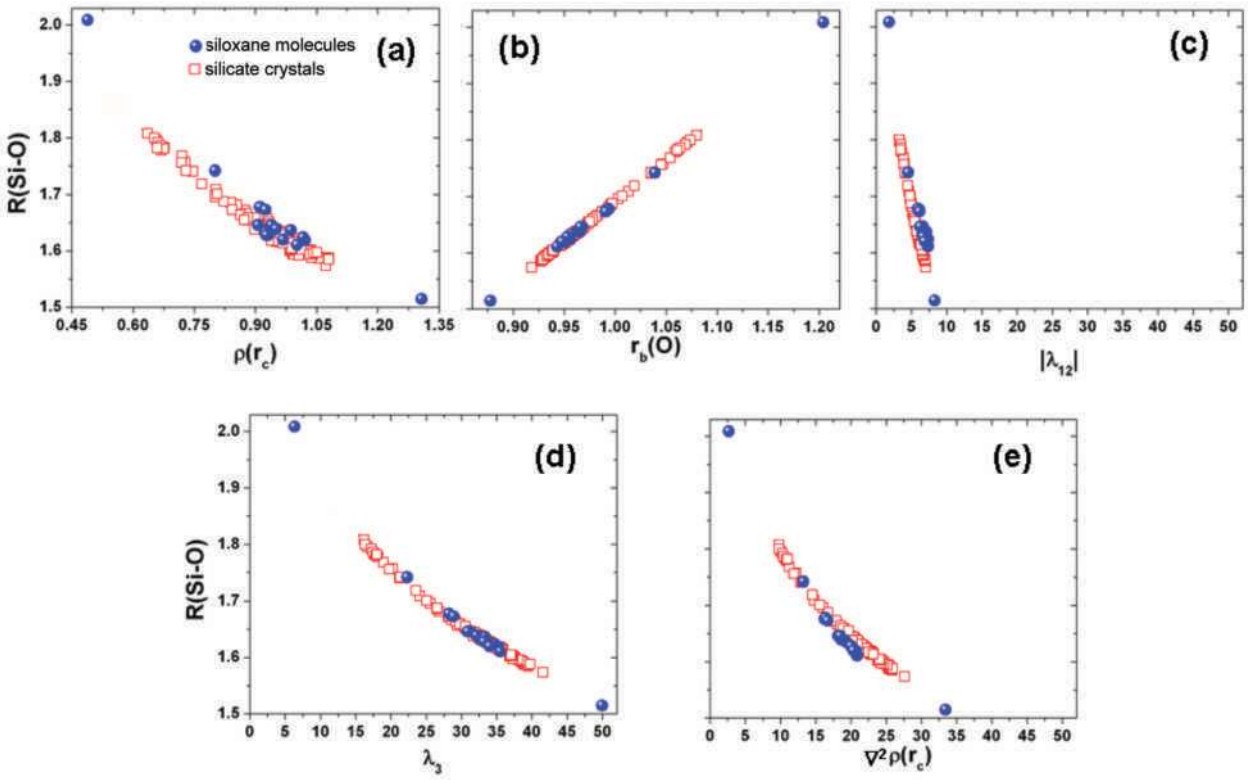

FIGURE 10. A comparison of the bond critical point properties calculated for silicate crystals displayed in Figure 4 (open red squares) with the bond critical point properties calculated for a variety of geometry optimized siloxane molecules (blue spheres) (Gibbs et al. 1998). In preparing these scatter diagrams, it was discovered that the bcp properties for the disiloxane molecule were incorrectly reported in Table 1 of Gibbs et al. (1998). They should read $\rho(\mathbf{r}_c) = 0.906$ e/Å^3, $r_b(O) = 0.966$ Å, $|\lambda_{1,2}| = -6.212$ Å^5, $\lambda_3 = 30.88$ e/Å^5, $\nabla^2\rho(\mathbf{r}_c) = 14.46$ e/Å^5, and $H(\mathbf{r}_c) = 0.238$ a.u.

ties for silicate crystals and representative siloxane molecules, provide support for the assertion that molecules are well-suited as models for studying the Si-O bonded interactions, reactions, and silica dissolution (cf. Lasaga and Gibbs 1990; Casey et al. 1990; Pelmenschikov et al. 2000; Du et al. 2003; Criscenti et al. 2006; Wojdel et al. 2006; Nangia and Garrison 2008). In addition, the experimental ^{IV}Si-O bridging bond lengths and the Si-O-Si angles observed for the bulk of the known silica polymorphs fall within ~4 kJ/mol of the minimum of a potential energy surface calculated for the $H_6Si_2O_7$ molecule (Gibbs et al. 2001, 2008a). The properties calculated for the $H_{12}Si_5O_{16}$ molecule have also been found to be comparable with those observed and calculated for coesite (Rosso et al. 1999). By the same token, in a search for global and minimum energy structures for silica, using dynamical simulated annealing and quasi-Newtonian minimization strategies with a potential energy function determined for the $H_6Si_2O_7$ molecule and starting with a random structure arrangement of six SiO_2 formula units in an asymmetric unit cell with $P1$ symmetry, the structure of quartz, among a large number of potential silica structure types, was derived. Despite the assumption of $P1$ symmetry and starting with a random arrangement of Si and O atom, the quartz structure generated in the search exhibited space group $P3_221$ symmetry with cell dimensions $a = 4.97$ Å, $c = 5.39$ Å, Si-O bond lengths of 1.612 Å (2×) and an Si-O-Si angle of 145.0° (Boisen et al. 1999); this compares well with the experimental space group $P3_221$, cell dimensions, $a = 4.91$ Å, $c = 5.40$ Å, and Si-O bonds 1.602 Å, 1.614 Å, and Si-O-Si angle 143.7° (Kihara 1990), further evidence that the bonded interactions in quartz are largely molecular in nature and that quartz and the other silica polymorphs are bound by virtually the same forces that bind the Si and O atoms in siloxane molecules. In the preface to his elegant book *Solids and Surfaces*, Hoffmann (1988) states that "The theoretical concepts that have served solid state chemists well have not been molecular," but, for the most part, they have been such empirical concepts as "ions (electrostatic forces, Madelung energies)" with "a certain size (ionic radii, packing considerations)." He continues by stating that these simple concepts have been "applied by solid state chemists even in cases of substantial covalency." With these observations, he posits the question "What can be wrong with an idea that works, and that explains structure and properties? What is wrong, or can be wrong is that the application of such concepts may draw that field, that group of scientists, away from the heart of chemistry. The heart of chemistry, let there be no doubt, is the molecule!"

BONDED RADII OF Si AND O

Despite the compilation of a highly cited empirical set of "effective" ionic and crystal radii, Shannon and Prewitt (1969) were careful to point out that their study had not resolved the important question regarding the absolute sizes of the cations and anions. The question was considered to be particularly relevant to the crystal chemistry of ionic materials because, if the sizes of the effective ions were real and absolute, then the structures of many ionic materials could be pictured authentically as close packed arrays of large oxide anions with the smaller cations

tucked away in the available tetrahedral and octahedral voids. But, notwithstanding the fact that their effective radii reproduce bond lengths to typically within ~0.01 Å, they cautioned that the actual sizes of the radii should not be considered too rigidly in deriving a physical picture of an ionic solid, particularly given that they were not derived from ED distributions. At that time, ED distributions were scarce in number and too poor in accuracy for the determination of the absolute sizes of the atoms. Assuming that the real radius of an O atom is given by the distance between the nucleus of the atom and the minimum in ED between the atom and the nucleus of a bonded metal atom [in effect, the bonded radius, r_b(O), of the atom], they asserted that the bonded radius of the O atom may not be constant, but that it may vary, depending on the type of metal atom to which it is bonded. Their assertion has since been borne out by the publication of accurate experimental and calculated ED distributions and r_b(O) values for a large number of silicates and oxides. As reported by Gibbs et al. (2001) for first and second row metal (M) atoms bonded to O, r_b(O) does indeed depend upon the properties of the M atoms to which the O atom is bonded; it also correlates with the M-O bond length, increasing progressively with increasing M-O bond length from 0.65 Å when bonded to N (the atomic radius of the O atom) to 1.50 Å when bonded to Na (comparable with the ionic radius of the oxide anion) (Gibbs et al. 2001). The bonded radii of the M atoms also increase in size with bond length but to a lesser extent than r_b(O). It is also noteworthy that the bonded radius of the H atom bonded to first and second row atoms also depends on the properties of the atom to which it is bonded; it increases systematically from ~0.3 Å when bonded to N to ~0.8 Å when bonded to Na (Gibbs et al. 1992).

For the silica polymorphs, r_b(O) = ~0.95 Å for the two-coordinated ^{II}O atoms in coesite and ~1.10 Å for the three-coordinated ^{III}O atom in stishovite. However, these radii are not only substantially smaller than the Shannon and Prewitt (1969) two- and three-coordinated crystal radii, 1.21 and 1.22 Å, respectively, for the oxide anion, but also the difference between the crystal radii is substantially smaller than the difference between the bonded radii. In contrast, the bonded radius of the Si atom in coesite is ~0.66 Å, while it is ~0.68 Å in stishovite compared with the crystal radii for four- and six-coordinated Si, 0.40 and 0.54 Å, respectively. On the basis of the ED distribution, it is the bonded radius of the O atom, not the crystal radius of the Si atom that changes substantially with the increasing coordination number of Si.

Furthermore, the bonded radius of an individual O atom is not single-valued. A given O atom may display two or more different radii, depending on the kinds of metal atoms to which it is bonded. For example, the three nonequivalent O atoms in danburite, $CaB_2Si_2O_8$ (Downs and Swope 1992) are each bonded to three different kinds of metal atoms, B, Si, and Ca, with average experimental M-O bond lengths of 1.47, 1.62, and 2.44 Å, respectively. Rather than displaying a single radius, each O atom displays a bonded radius of ~1.00 Å along the B-O bond path, a radius of ~ 0.94 Å along the Si-O bond path and a radius of ~1.23 Å along the Ca-O bond path, a result that substantiates the claim of O'Keeffe and Hyde (1981) that the radius of an atom like O is not single-valued. As they point out, the use of the term "radius" for an O atom implies that the size of the atom is the same in all directions, which they consider to be "clearly absurd." The bond path closely parallels the line between two bonded atoms in the bulk of the materials studied such that the bonded radius is effectively measured along the bond length, a result that reflects on the stability of the bonded interactions (Bader 1990). The variability of the r_b(O) with the type of atom to which it is bonded is also consistent with the observation that r_b(O) correlates with the electronegativity difference between bonded M and O atoms; the greater the difference and the greater closed-shell interaction, the larger the bonded radius for the O atom (Feth et al. 1993). As is well known, the Shannon and Prewitt (1969) crystal radii have been used with considerable success in the generation of bond lengths, structure field diagrams, and the modeling of ion conductivity, defects, diffusion and site preferences, among other things, in advancing the understanding of oxide crystal chemistry (Prewitt 1985). As observed by O'Keeffe and Hyde (1981), this is expected, given that the Shannon and Prewitt (1969) table of radii is in effect a table of average M-O bond lengths. After all, experimental bond lengths were used in the compilation of the radii, assuming a given radius for an oxide anion with a given coordination number and the Bragg (1920) additive rule. Given that average bond lengths were used to construct the radii, assuming a given radius for the oxide anion, it is clear that one could use any radius of interest for the oxide anion and compile a set of workable radii. For example, if one used the strategies devised by Shannon and Prewitt (1969) and Bragg's (1920) atomic radius for the O atom (0.65 Å), for example, one would obtain another set of empirical radii that would be comparable with Slater's (1964) universal radii, and it would work as well as the Shannon and Prewitt (1969) radii in predicting bond lengths. But, unlike the Shannon and Prewitt (1969) radii, the resulting radii would be universal in their application, serving to predict bond lengths for oxides, sulfides, metals and molecules alike, regardless of whether bonded interactions were ionic, covalent, or metallic in nature. Clearly, it goes without saying that the fact that a set of ionic radii works and provides a basis for understanding properties and crystal chemistry says little about the actual sizes of the atoms themselves. As the radius of an ion is not constant, it can be argued that it is the bond length (an observable), not the radii of the atoms that should be considered when conjecturing whether one bonded interaction (rather than a given atom) in a structure can be replaced by another or whether one structure is favored over another in a structural field map based on bond length. After all, it is the bond length that is connected to the energy and the stability of a bonded interaction, not the radii of the atoms comprising the bonded interaction. It is clear, however, that the main reason that crystal radii work and that they have been so useful in crystal chemistry in understanding a wide range of properties is that radii are correlated on a one-to-one basis with the average experimental bond lengths used in their derivation.

In the modeling of the structures of quartz and coesite as a function of pressure, r_b(Si) and r_b(O) were found to decrease slightly with increasing pressure. Over the pressure range studied, r_b(O) was found to decrease from 0.95 to 0.90 Å, while r_b(Si) decreased substantially less from 0.66 to 0.65 Å. Given that r_b(O) is more dependent on the Si-O bond length and the coordination number of Si than the bonded radius of the Si atom, the greater

decrease of the r_b(O) with increasing pressure may be expected. The decrease in r_b(Si) atom with increasing pressure, albeit small, suggests that the O atom is more compressible than the Si atom, at least along the Si-O bond path (Gibbs et al. 1999, 2000; Prencipe and Nestola 2007). The greater compressibility of the O atom is consistent with Ida's (1976) conclusion that the compressibilities of Mg, Fe, and Si are negligibly small and that the compressibilities of silicates in the mantle are dictated in large part by the greater compressibility of the O atom. Miyamoto and Takeda (1980) and Matsui et al. (1982) reached a similar conclusion on the basis of the molecular dynamics determined for selected Mg-silicates.

Si AND O NET ATOMIC CHARGES

Bader (1985) postulated that an atom in a material consists of a nucleus and its associated electrons that are collectively enclosed within a surface, $S(\mathbf{r})$, that exhibits a zero flux property, a surface that is not crossed by any trajectories of the gradient field vectors of $\rho(\mathbf{r})$. This condition is satisfied when the inner product $\nabla\rho(\mathbf{r})\cdot\mathbf{n} = 0$ holds, where $\mathbf{n}$ is a unit vector oriented perpendicular to $S(\mathbf{r})$ (see Fig. 1 in Bader 1985). The region of space enclosed by $S(\mathbf{r})$ is referred to as the basin of the atom. By integrating the ED over the range of an atomic basin, the number of electrons in the basin can be determined. The net atomic charge of an atom, q, is obtained by simply summing the nuclear charge of the atom and the electronic charge associated with the number of electrons in the basin.

A careful study of the structures and topologies of the ED distributions for disiloxane and several related molecules (Gillespie and Johnson 1997), resulted in a geometry optimized disiloxane molecule with an Si-O bond length of 1.621 Å, compared with the experimental length of 1.634 Å, and an Si-O-Si angle of 148.6°, compared with the experimental angle of 144.1°. Considering the very compliant nature of the angle, the agreement between the experimental and model structures is considered to be good. The short Si-O bond compared with the sum of the single covalent radii for Si and O, 1.92 Å, the large net atomic charges conferred on the Si and O atoms, q(Si) = +3.05 e and q(O) = –1.52 e, respectively, and the wide Si-O-Si angle were concluded to be a direct consequence of the highly ionic character of the Si-O bond. However, given the compliant nature of the Si-O-Si angle, it is difficult to understand, in light of the large net charges on the Si atoms, why the angle is bent rather than straight (Geisinger and Gibbs 1981; O'Keeffe and McMillan 1986).

An integration of the ED distribution over the basins of the ^{IV}Si and ^{II}O atoms for quartz resulted in even larger net charges of $q(^{IV}\text{Si})$ = +3.20 e and $q(^{II}\text{O})$ = –1.60 e (Gibbs et al. 1999). The net charges calculated for the ^{VI}Si and ^{III}O atoms in stishovite are even larger, $q(^{VI}\text{Si})$ = +3.39 e and $q(^{III}\text{O})$ = –1.69 e, as expected, given the larger coordination numbers of the Si and O atoms in stishovite (Kirfel et al. 2001). Prencipe and Nestola (2007) found that the ^{IV}Si atom in beryl, has a q-value of +3.2, in close agreement with that found for quartz. The large net charges obtained in these studies are consistent with charges inferred from maxima in the experimental deformation [$\Delta\rho(\mathbf{r})$] map reported for quartz and stishovite (Cohen 1994), charges of ~ +4 on Si and ~ –2 on O. The large charges are also consistent with the fully ionic electrostatic potential energy model used by Smyth (1989) to locate potential sites for hydroxyl substitution and to estimate oxygen isotope fractionation in silicate and oxide minerals. Clearly, a highly ionic model for the Si-O bond contradicts Pauling's (1939) long held view that the bond is intermediate in character between ionic and covalent, rather than highly ionic. These large charges conform with the convictions of Prencipe et al. (2002) and Prencipe and Nestola (2007), who believe that an ionic picture of the Si-O bond is more appropriate than a covalent one.

It is well known that the net atomic charges conferred on the atoms of quartz, coesite, and stishovite are substantially larger than those obtained by X-ray diffraction methods. For example, spherical κ-refinements of single-crystal X-ray diffraction data sets resulted in a –0.74 e net charge on the ^{II}O atoms of coesite (Downs 1995) and –0.86 e net charge on the ^{III}O atoms of stishovite (Hill et al. 1983), substantially smaller than the charges obtained in the virial partitioning of the ED. A careful multipole study of accurate structure factors for synthetic quartz by Stewart et al. (1980) yielded smaller charges with a net residual charge of +1.0 e conferred on the pseudoatom Si atom and charge of –0.5 e conferred on the pseudoatom O atom. On the basis of these charges and electronegativity considerations, it was concluded that the Si-O bond in quartz is 25% rather than 100% ionic.

In a recent assessment of Voronoi deformation ED density charges, Guerra et al. (2004) concluded that net atomic charges are much too large in certain cases, conferring excessive ionic character on a variety of covalent bonds. (See also Haaland et al. 2000.) As a case in point, the net atomic charges (~3.5 e) conferred on the P atoms of PO_4 tetrahedral oxyanions in the $AlPO_4$-15 molecular sieve framework structure, determined in a careful ED study, are even larger than those conferred on the Si atom in quartz (Aubert et al. 2003). In a rebuttal of the criticisms of the large net charges, Bader and Matta (2004) pointed out that the net charge conferred on an atom is the expectation value of the number operator that counts the average number of particles within a given spatial region, and as such, the number of electrons in the basin of an atom is an observable. This is true, but the question remains whether all of the electrons "belonging" to a given atom are always contained within the basin of the atom (Parr and Yang 1989). Furthermore, it is difficult to rationalize the experimental Si-O-Si angle of cristobalite, 146.5° (Gibbs et al. 1999) and the bent 148.6° angle for the disiloxane molecule with net charges of +3.05 and –1.72 e conferred on the Si and O atoms. Nonetheless, the larger net charges conferred on the ^{VI}Si and ^{III}O atoms of stishovite relative to those conferred on the ^{IV}Si and ^{II}O atoms in quartz are consistent with the greater ionic character of the ^{VI}Si-^{III}O bond. This result suggests that the relative magnitudes of the net charges are correct but perhaps their absolute magnitudes may be too large, as concluded by Guerra et al. (2004).

In the study of the quartz structure as a function of pressure, the magnitude of net charge conferred on O was found to decrease slightly from –1.600 to –1.595 e with increasing pressure over the pressure range studied, 0.0 to 18 GPa. The magnitudes of q(O) for the zero pressure model structure of coesite also decrease from –1.606 to –1.595 e with decreasing Si-O bond length and Si-O-Si angle. In contrast, the magnitudes of the net charges conferred on the O atoms involved in the narrower Si-O-Si angles

(O2 and O5) actually increase with increasing pressure, whereas the magnitudes of net charges on the remaining O atoms, (O1, O3, and O4) actually decrease as observed for the O atoms of quartz. These conflicting results suggest that little can be said about how q(O) changes with increasing pressure in the case of coesite. The magnitude of the experimental atomic charge for the O atom in stishovite is slightly larger, q(O) = –1.69 e, than that for either quartz or coesite, a result that is expected given the longer Si-O bond length, the smaller value of $\rho(\mathbf{r}_c)$, and the larger coordination number of the Si atom in stishovite (Kirfel et al. 2001). The bcp properties, the larger q(Si) and the smaller q(O) values, the larger bonded radius of the oxide anion and the larger coordination number of the Si atom in stishovite, are consistent with the argument that the Si-O bond in stishovite is more ionic than it is in either quartz or coesite. The ionicities, $\kappa_{Si\text{-}O} = \frac{1}{2}|q(\mathrm{Si})/\nu_{Si} - q(\mathrm{O})/\nu_O|$ where ν_{Si} and ν_O are the valences of Si and O, respectively (Zwijnenburg et al. 2002), calculated for the Si-O bonds in quartz ($\kappa_{Si\text{-}O}$ = 0.80) and stishovite ($\kappa_{Si\text{-}O}$ = 0.84) are likewise consistent with the assertion that the bonds in stishovite are more ionic than those in quartz.

The elusive character of the Si-O bond

Given the vast amount of literature written about silicates and siloxanes, it may come as a surprise that a general consensus has yet to be reached regarding the character of the Si-O bond. Workers like Smyth (1989), Cohen (1994), Gillespie and Johnson (1997), Prencipe et al. (2002), and Prencipe and Nestola (2007) believe that the bond is largely ionic; others like Harrison (1978) and Stewart et al. (1980) believe that it is predominately covalent, whereas others like Pauling (1939) and Gibbs et al. (1999) believe that it is intermediate in character between ionic and covalent. Given these divergent viewpoints, it is clear that the character of the Si-O bond is an elusive subject (Catlow and Stoneham 1983; Gibbs et al. 1994), shrouded in mystery and contradictory results. A fully ionic model for quartz, consisting of Si^{+4} and O^{-2} ions, gives a reasonably good fit to the dielectric properties and the cohesive energy (Sanders et al. 1984; Jackson and Gordon 1988; Burnham 1990); yet, an intermediate model with Si^{+2} and O^{-1} ions gives a better fit to the photon frequencies and to Phillip's (1970) dielectric model (Vempati and Jacobs 1983; Jackson and Gordon 1988) and a covalent model with residual charges of +1 on Si and –0.5 e.u. is consistent with the ED distribution observed for quartz (Stewart et al. 1980).

With the advent of the robust theory of Bader (1990) and his colleagues for characterizing the topology of ED distributions for molecules and crystals, it has been demonstrated that a bonded interaction can be classified in terms of the bond critical point properties, the local potential density, $V(\mathbf{r}_c)$, and the local kinetic energy density, $G(\mathbf{r}_c)$. As a basis for the classification, Bader and Essén (1984) observed that the kinetic density, $G(\mathbf{r})$ in a.u., and its components may be related directly to the inner product of the gradients of the orbital electron densities, ρ_i, and their occupation numbers, n_i, by the expression:

$$G(\mathbf{r}) = \tfrac{1}{8}\Sigma_i\, n_i\, [\nabla\rho_i(\mathbf{r})\cdot\nabla\rho_i(\mathbf{r})/\rho_i(\mathbf{r})]$$

where the summation is completed over the natural spin-orbital components (Parr and Yang 1989). With a determination of $G(\mathbf{r})$, $V(\mathbf{r})$ can be determined once $\nabla^2\rho(\mathbf{r})$ is known, using the local form of the virial theorem, $V(\mathbf{r}) = \frac{1}{4}\nabla^2\rho(\mathbf{r}) - 2G(\mathbf{r})$ (Bader 1990). With values $\rho(\mathbf{r}_c)$, $\nabla^2\rho(\mathbf{r}_c)$, and $G(\mathbf{r}_c)$, Bader and Essén (1984) introduced a classification of bonded interactions based on: (1) the sign of $\nabla^2\rho(\mathbf{r}_c)$; (2) whether the local kinetic energy per electronic charge, $G(\mathbf{r}_c)/\rho(\mathbf{r}_c)$, is greater or less than unity; and (3) whether the value of $\rho(\mathbf{r}_c)$ is > or < 1.0 e/Å^3, each evaluated at the bond critical point of a bonded interaction. They asserted that a bonded interaction is shared (covalent) when the value of $\nabla^2\rho(\mathbf{r}_c)$ is negative, $\rho(\mathbf{r}_c)$ is greater than ~1.0 e/Å^3 and $G(\mathbf{r}_c)/\rho(\mathbf{r}_c)$ is less than unity, and that it is closed shell (ionic) when $\nabla^2\rho(\mathbf{r}_c)$ is positive, $\rho(\mathbf{r}_c)$ is smaller than ~1.0 e/Å^3 , $G(\mathbf{r}_c)/\rho(\mathbf{r}_c)$ is greater than unity and $\mathbf{r}_c$ is located relatively far from the nodal surface [$\nabla^2(\mathbf{r}) = 0\ \forall\ \mathbf{r}$] of the Laplacian. But when $\mathbf{r}_c$ is located in close proximity to the surface, the bonded interaction is asserted to be an intermediate interaction, the closer $\mathbf{r}_c$ is to the surface, the more shared the interaction. It is noteworthy that the net atomic charges conferred on the bonded atoms were not expressly considered in the classification.

As the $\nabla^2\rho(\mathbf{r}_c)$ values for the silicates considered in Figure 6 are all positive, each of the Si-O bonded interaction qualifies either as a closed-shell or an intermediate interaction, depending on the distance that $\mathbf{r}_c$ is from the nodal surface of the Laplacian. In an earlier study of several siloxane molecules, Gibbs et al. (1997) measured the distances between the nodal surfaces and $\mathbf{r}_c$ for the molecules and found that they decrease systematically as the Si-O lengths decrease and $\rho(\mathbf{r}_c)$ and $\nabla^2\rho(\mathbf{r}_c)$ each increases in value. The distance between $\mathbf{r}_c$ and the nodal surface was found be ~0.60 Å for the ^{VIII}Si-O bonded interaction of the $H_{12}{}^{VIII}SiO_8$ molecule, ~0.40 Å from the surface for the ^{VI}Si-O bonded interaction of the $H_8{}^{VI}SiO_6$ molecule to ~0.15 from the surface for the ^{IV}Si-O bond interaction of the $H_4{}^{IV}SiO_4$ molecule. On the basis of the Bader and Essén classification, the ^{VIII}Si-O bonded interaction qualifies as a closed-shell ionic interaction [$\rho(\mathbf{r}_c)$ = 0.47 e/Å^3; $\nabla^2\rho(\mathbf{r}_c)$ = 6.16 e/Å^5], the ^{VI}Si-O bonded interaction qualifies as an intermediate interaction with a marginal component of closed-shell character [$\rho(\mathbf{r}_c)$ = 0.74 e/Å^3; $\nabla^2\rho(\mathbf{r}_c)$ = 15.78 e/Å^5] and the ^{IV}Si-O bonded interaction [$\rho(\mathbf{r}_c)$ = 0.94 e/Å^3; $\nabla^2\rho(\mathbf{r}_c)$ = 26.00 e/Å^5] qualifies as an intermediate interaction. Consistent with these results, the $G(\mathbf{r}_c)/\rho(\mathbf{r}_c)$ ratio increases from ~1.0 for the ^{VIII}Si-O interaction to ~2.7 for the ^{IV}Si-O interaction (Fig. 11) as the shared character of the bonded interactions increases in conformity with the decrease in the distance between the bond critical point and the Laplacian nodal surface and the decrease in the coordination number of Si (Gibbs et al. 2006b). Concomitant with this trend, $\nabla^2\rho(\mathbf{r}_c)$ increases from 6.16 to 26.00 e/Å^5 as the coordination numbers of the Si atoms of the siloxane molecules decrease from eight to four and as $\rho(\mathbf{r}_c)$ increases from 0.47 to 0.94 e/Å^3. The decrease in the coordination number and the increase in $\rho(\mathbf{r}_c)$ suggest that $\nabla^2\rho(\mathbf{r}_c)$ actually increases as the shared character of an intermediate bonded interaction increases. To establish whether this connection holds in general, the $\nabla^2\rho(\mathbf{r}_c)$ values, calculated for a large number of M-O bonded interactions involving first and second row M atoms, were plotted with respect to the $\rho(r_c)$ values calculated for the interactions (Fig. 12) (Gibbs et al. 2001, 2008a). As displayed by the figure, $\nabla^2\rho(\mathbf{r}_c)$ increases linearly with $\rho(r_c)$ for each of the bonded interactions, the larger the value of $\rho(r_c)$, the smaller the coordination number of the M atoms and

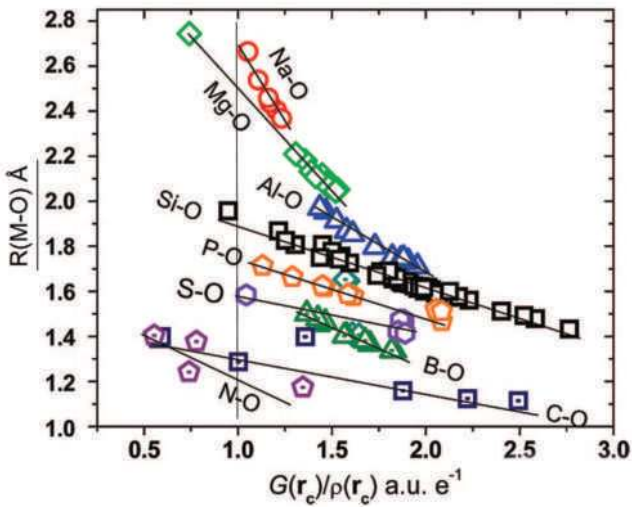

FIGURE 11. Scatter diagram of the bond lengths, R(M-O) Å, determined for many silicates, oxides, and representative molecules plotted with respect to $G(\mathbf{r}_c)/\rho(\mathbf{r}_c)$ a.u./e for first and second row M atoms bonded to O. For each of the bonded interactions, as $G(\mathbf{r}_c)/\rho(\mathbf{r}_c)$ increases with decreasing bond length, the coordination numbers of the M atoms decrease and $\rho(\mathbf{r}_c)$ increases. For example, as the $G(\mathbf{r}_c)/\rho(\mathbf{r}_c)$ ratio increases for the B-O bonded interactions from ~1.5 to ~2.0 a.u./e, the coordination number of B decreases from 4 to 3 and the B-O bond lengths decrease from R(^{IV}B-O) = ~1.45 Å to R(^{III}B-O) = ~1.35 Å. For the Al-O bonded interactions, as the ratio increases from ~1.5 to ~2.0 a.u./e, the coordination number decreases from 6 to 4 and the Al-O bond lengths decrease from R(^{VI}Al-O) ~ 1.95 Å to R(^{V}Al-O) ~ 1.85 Å to R(^{IV}Al-O) ~ 1.75 Å . For the Si-O bonded interactions, as the ratio increases from ~1.0 to ~2.7 a.u./e, the coordination number decreases from 8 to 4 and the Si-O bond lengths decrease from R(^{VIII}Si-O) ~ 2.01 Å to R(^{VI}Si-O) ~ 1.77 Å to R(^{IV}Si-O) ~ 1.62 Å. As the ratio for the C-O bonded interactions increases from ~0.5 to ~2.5 a.u./e and the coordination number decreases from 4 to 1 as the C-O bond lengths decrease from R(^{IV}C-O) ~ 1.39 Å to R(^{III}C-O) ~ 1.29 Å to R(^{II}C-O) ~ 1.16 Å to R(^{I}C-O) ~ 1.12 Å. With exceptions of R(Na-O) and R(Mg-O), as R(M-O) decreases, the local energy density is negative and $H(\mathbf{r}_c) = G(\mathbf{r}_c) + V(\mathbf{r}_c)$ decreases, and the shared character of the bonded interactions are indicated to increase (see Gibbs et al. 2006b).

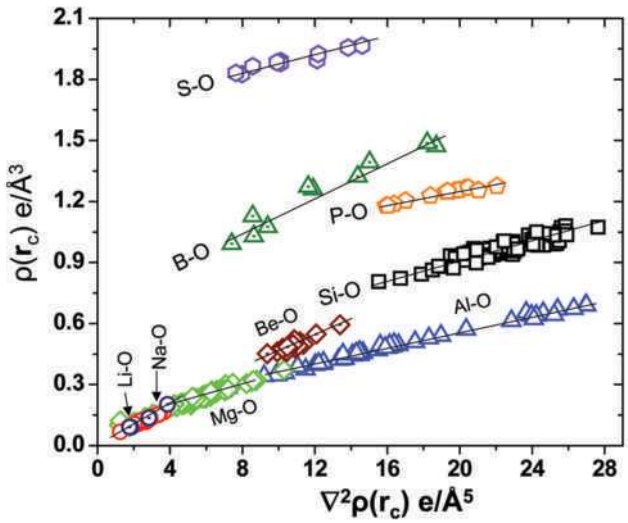

FIGURE 12. Scatter diagram of $\rho(\mathbf{r}_c)$ plotted with respect to $\nabla^2\rho(\mathbf{r}_c)$, calculated for first and second row M atoms bonded to O. The bcp properties used to construct these plots were taken from the properties of structures used to construct Figures 17a and 17b published by Gibbs et al. (2008a). Li-O is plotted as blue circles, Na-O as red circles, Mg-O as light green diamonds, Be-O as brown triangles, Al-O as blue triangles, Si-O as black squares, P-O as orange pentagons, B-O as dark green triangles, and S-O as violet hexagons.

the larger the value of $\nabla^2\rho(\mathbf{r}_c)$. Furthermore, when the bond lengths for the bulk of these interactions are plotted with respect to the ratio $G(\mathbf{r}_c)/\rho(r_c)$ (Fig. 11), the ratio increases linearly as the bond length decreases, $\rho(r_c)$ increases and the coordination numbers of the M atoms decrease, as observed for Si-O bonded interactions. The Bader-Essén (1984) assertion that a bonded interaction qualifies as a shared interaction when the value of $G(\mathbf{r}_c)/\rho(\mathbf{r}_c)$ is less than unity and a closed-shell one when it is greater than unity is not borne out by the trends displayed for the non-transition M-O bonded interactions (Fig. 11) or those displayed for a number of transition M-O bonded interactions observed for carboxylate Fe bridged and butterfly complexes and Mn and Co containing organometallic coordination polymers (Clausen et al. 2008; Gibbs et al. 2008b). The trends suggest, at least for M-O bonded interactions, that relatively large positive $G(\mathbf{r}_c)/\rho(\mathbf{r}_c)$ ratios are compatible with a non-trival component of shared character, the larger the ratio for a given M-O bonded interaction, the more shared the interaction. The trends in Figure 12 show, at least for the M-O bonded interactions, that when the value of $\nabla^2\rho(\mathbf{r}_c)$ is positive, $\rho(r_c)$ increases as the shared character of the bonded interactions increases, particularly given that the local total energy density values for the bulk of the bonded interactions are negative (except Li-O, Na-O, and Mg-O bonded interactions as discussed above) and that each decreases with the increasing value of $\rho(r_c)$. It also suggests that ^{VI}Si-O and ^{IV}Si-O are both intermediate bonded interactions, despite their large $\nabla^2\rho(\mathbf{r}_c)$ values, with the ^{IV}Si-O bonded interaction possessing a slightly greater component of shared character than the ^{VI}Si-O bonded interaction.

In sharp disparity, the large net charges conferred on the Si (+3.2 e) and O (–1.6 e) atoms of quartz, obtained by integrating the ED over the range of the basins for the two atoms, indicate that the Si-O bond is highly ionic, whereas the pseudoatom charges conferred on Si (+1.0 e) and O (–0.50 e) atoms in the multipole X-ray refinement of the ED distribution for quartz indicate that the bond is intermediate in character with a substantial component of covalent character. In an important exploration of the impact of ionicity on the structure and stability of quartz, Jackson and Gordon (1988) completed a careful modeling of the structure and the equation of state with the fully ionic modified electron gas MEG-I model to explore the extent to which the experimental properties for the silica polymorph conform with those predicted for a fully ionic model structure. The Si-O distances (1.54 Å), the Si-O-Si angle (163°), and the isothermal bulk modulus (300 GPa) generated by the MEG-I quartz model were found to depart substantially from the experimental values (1.61 Å, 145°, and 37 GPa, respectively). It is notable that the calculated MEG-I bulk modulus is of the same order as that observed for stishovite (313 GPa), one of the most incompressible oxides known, whereas quartz is one of the most compressible oxides. The huge difference between the experimental bulk modulus of quartz and that calculated with the fully ionic model (about an

order of magnitude larger than that observed) shows that a highly ionic structure with highly charged Si and O atoms utterly fails in the modeling of the elastic properties, demonstrating, beyond a shadow of doubt, that a strongly ionic model for quartz is unsatisfactory (Gibbs et al. 1999, 2000). Of equal importance, the deformation ED $\Delta\rho(\mathbf{r})$ and the ELF distributions generated for quartz and the other silica polymorphs display substantial accumulations of ED in both the lone pair and bond pair regions of the Si-O bond vectors, features that are clearly not expected for an ionic bond and a structure that contains highly charged Si and O ions with spherical ED distributions (Gibbs et al. 2003a, 2003b, 2005a, 2008a). Last, the close proximity of the ^{IV}Si-O bond critical point with the nodal plane of the Laplacian and the negative value of $H(\mathbf{r}_c)$ serve as evidence that the Si-O bond has a nontrivial component of shared character (Cremer and Kraka 1984). Taken together, these features are considered to satisfy criteria that qualify the bond interaction as a bond of intermediate character. The one shortcoming with this assertion is the large net atomic charges that are conferred on the Si and O atoms in quartz, charges that are clearly difficult to square with the features displayed in the $\Delta\rho(\mathbf{r})$ and ELF maps and the small bulk modulus observed for quartz. Clearly, an explanation for these charges is required. One possible explanation is that all of the electrons that "belong" to the Si and O atoms in the silica polymorphs and the $H_6Si_2O_7$ molecule are not contained within the basins of the atoms (Parr and Yang 1989; Guerra et al. 2004). If true, then this would explain the large charges. A similar argument may also be used to explain the large charges conferred on the P atoms of the molecular sieve, $AlPO_4$-15.

Concluding remarks

The optimization of the structures for the silica polymorphs as a function of pressure with first-principles density functional theory and the generation of model structures that rival the accuracy of experimental ones have demonstrated that theory and software have evolved to the level where it is now possible to generate accurate structures for a wide range of minerals as a function of pressure and composition, and to determine their equations of state (Demuth et al. 1999). In addition, it is also possible to model physical and surface properties, templating, and catalysis and the reactivity of materials (Panero and Stixrude 2004; Brodholt and Vocadlo 2006; Catlow et al. 2005; Woodley and Catlow 2008). Also, as the ED distribution for a ground state mineral suffices for the determination of all of its properties (Parr and Yang 1989), it is an ideal medium for studying bonded interactions. Bond paths and the bond critical point properties calculated for the ED distributions for siloxane molecules are comparable with those observed for the silica polymorphs, a result that indicates that the forces that govern the structures and properties of the silica polymorphs are largely short-ranged and molecular in nature rather than being long-ranged and strongly ionic.

The success of first-principles computational quantum mechanical calculations in the determination of structures and ED distributions that are in close agreement with experimental structures and distributions for the silica polymorphs bodes well for future first-principles studies of Earth materials, their structures, properties, and reactivity. Also, as observed by Gibbs et al. (2008a), the calculations are not only expected to assist in the development and interpretation of experimental results, but they will also provide a deeper understanding of crystal chemistry, properties, mineralogical processes, and chemical reactions beyond the unobservables embodied in Pauling's rules, bond strength relationships, and ionic and crystal radii, thereby enriching the fields of mineralogy and geochemistry, particularly when a given property or reaction is studied for a variety of chemically related materials like the silicates (Gibbs et al. 2008a, 2008c), transition metal sulfides (Gibbs et al. 2005b, 2007) and arsenites (Gibbs et al. 2009). In short, if mineralogists and geochemists persist in their study of minerals, their properties and relationships within the framework of empirical parameters like ionic radii, bond strength and electrostatic potential and forces and do not include first-principles quantum mechanical calculations and the study of ED distributions, then it questionable whether our understanding of the crystal chemistry and the properties of minerals in their natural environments will advance much beyond that of last century.

As a final point, software is currently being written in our laboratories to evaluate the potential, kinetic, and the total energy densities globally with the goal of obtaining a more comprehensible understanding of the bonded interactions throughout a crystal rather than just at its bond critical points (Cremer and Kraka 1984). Furthermore, energy density isosurface maps will be generated for crystals that have been determined over a range of pressures as a means of monitoring how the densities vary globally throughout a crystal as a function of pressure. By locating those regions where $H(\mathbf{r}) < 0$, that are stabilized relative to those where $H(\mathbf{r}) > 0$, we may expect to pinpoint those regions in the structure where the bonded interactions are stabilized relative to those that are destabilized (Tsirelson 2002). This information is expected to provide important insight into how the structure of the crystal responds to pressure and how the bonded interactions might be disrupted at the atomic level upon approaching a phase transformation. The information may also improve our understanding of the connection between the bonded interactions and the equation of state of the crystal at the atomic level. Also, calculations for topologically equivalent but chemically different structures like forsterite and fayalite are expected to shed light on the impact on the stability of a structure at the atomic level accompanying the replacement of one atom by another.

Acknowledgments

The National Science Foundation and the U.S. Department of Energy are thanked for supporting this study with Grants EAR-0609885 (N.L.R. and G.V.G.), EAR-0609906 (R.T.D.), and DE-FG02-97ER14751 (D.F.C.). K.M.R. acknowledges a grant from the U.S. Department of Energy (DOE), Office of Basic Energy Sciences, Geoscience Division and computational facilities and support from the Environmental Molecular Sciences Laboratory (EMSL) at the Pacific Northwest National Laboratory (PNNL). The computations were performed in part at the EMSL at PNNL. The EMSL is a national scientific user facility sponsored by the U.S. DOE Office of Biological and Environmental Research. PNNL is operated by Battelle for the DOE under contract DEAC06-76RLO 1830. G.V.G. owes a debt to his good friend and colleague Richard Bader for forging his elegant theory on the topology of electron density distributions and in particularly for his patience in responding to his many emails seeking advice and help in understanding the science. We are pleased to acknowledge Mauro Prencipe of the University of Torino for reviewing the manuscript and for making several important suggestions that clearly improved the manuscript. We also thank a second reviewer who urged that we make a statement at the beginning of the manuscript, giving the reader an overview of the contents of the paper. It was a good idea and we thank the reviewer for the suggestion. Color in figures courtesy of MSA Color Fund.

REFERENCES CITED

Alvarez, S., Hoffmann, R., and Mealli, C. (2009) A bonding quandary or a demonstration of the fact that scientists are not born with logic. Chemistry—A European Journal, in press.

Angel, R.J., Shaw, C.S.J., and Gibbs, G.V. (2003) Compression mechanisms of coesite. Physics and Chemistry of Minerals, 30, 167–176.

Aubert, E., Porcher, F., Souhassou, M., and LeComte, C. (2003) Characterization of intra-framework and guest/host interactions in the $AlPO_4$-15 molecular sieve by charge-density analysis. Acta Crystallographica, B59, 689–700.

Bader, R.F.W. (1985) Atoms in molecules. Accounts of Chemical Research, 18, 9–15.

——— (1990) Atoms in Molecules. Oxford Science Publications, U.K.

——— (1998) A bond path: A universal indicator of bonded interactions. Journal of Physical Chemistry A, 102, 7314–7323.

——— (2008) There are no bonds—Only bonding! Frontiers in Chemistry Series: Case Western Reserve University, McMaster University.

Bader, R.F.W. and Essén, H. (1984) The characterization of atomic interactions. Journal of Chemical Physics, 80, 1943–1960.

Bader, R.F.W. and Matta, C.F. (2004) Atomic charges are measurable quantum expectation values: A rebuttal of criticisms of QTAIM charges. Journal of Physical Chemistry A, 108, 8385–8394.

Bader, R.F.W., Slee, T.S., Cremer, D., and Kraka, E. (1983) Description of conjugation and hyperconjugation in terms of electron distributions. Journal of the American Chemical Society, 105, 5061–5068.

Bader, R.F.W., MacDougall, P.J., and Lau, C.D.H. (1984) Bonded and nonbonded charge concentrations and their relation to molecular geometry and reactivity. Journal of the American Chemical Society, 106, 1594–1605.

Berlin, T. (1951) Binding regions in diatomic molecules. The Journal of Chemical Physics, 19, 208–213.

Bianchi, R., Forni, A., and Oberti, R. (2005) Multipole-refined charge density study of diopside at ambient conditions. Physics and Chemistry of Minerals, 32, 638–645.

Boisen, M.B. and Gibbs, G.V. (1993) A modeling of the structure and compressibility of quartz with a molecular-potential and its transferability to cristobalite and coesite. Physics and Chemistry of Minerals, 20, 123–135.

Boisen, M.B., Gibbs, G.V., O'Keeffe, M., and Bartelmehs, K.L. (1999) A generation of framework structures for the tectosilicates using a molecular-based potential energy function and simulated annealing strategies. Microporous and Mesoporous Materials, 29, 219–266.

Bragg, W.L. (1920) The arrangement of atoms in crystals. The London, Edinburgh and Dublin Philosophical Magazine and Journal of Science, 40, 169–189.

Brodholt, J.P. and Vocadlo, L. (2006) Applications of density functional theory in the geosciences. MRS Bulletin, 31, 675–680.

Brown, I.D. and Shannon, R.D. (1973) Empirical bond-strength-bond-length curves for oxides. Acta Crystallographica Section A, 29, 266–282.

Burnham, C.W. (1990) The ionic model: Perceptions and realities in mineralogy. American Mineralogist, 73, 443–463.

Casey, W.H., Lasaga, A.C., and Gibbs, G.V. (1990) Mechanisms of silica dissolution as inferred from the kinetic isotope effect. Geochimica et Cosmochimica Acta, 54, 3369–3378.

Catlow, C.R.A. and Stoneham, A.M. (1983) Ionicity in solids. Journal of Physics C: Solid State Physics, 16, 4321–4338.

Catlow, R., Bell, R., Cora, F., French, S.A., Slater, B., and Sokol, A. (2005) Computer modeling of inorganic materials. Annual Reports on the Progress of Chemistry, Section A: Inorganic Chemistry, 101, 513–547.

Clausen, H.F., Overgaard, J., Chen, Y.S., and Iversen, B.B. (2008) Synchrotron X-ray charge density study of coordination polymer $Co_3(C_8H_4O_4)_4(C_4H_{12}N)_2(C_5H_{11}NO)_3$ at 16 K. Journal of the American Chemical Society, 130, 7988–7996.

Cohen, R.E. (1994) Silica, 369 p. Mineralogical Society, Washington, D.C.

Coulson, C.A. (1953) The Spirit of Applied Mathematics. Clarendon Press, Oxford.

——— (1955) The contributions of wave mechanics to chemistry. Journal of the Chemical Society, 2069–2084.

——— (1960) The present state of molecular calculations. Reviews of Modern Physics, 170–177.

Cremer, D. and Kraka, E. (1984) A description of the chemical bond in terms of local properties of electron density and energy. Croatica Chemica Acta, 57, 1259–1281.

Criscenti, L.J., Kubicki, J.D., and Brantley, S.L. (2006) Silicate glass and mineral dissolution: Calculated reaction paths and activation energies for hydrolysis of a Q^3 Si by H_3O^+ using ab initio methods. Journal of Physical Chemistry A, 110, 198–206.

Demuth, T., Jeanvoine, Y., Hafner, J., and Angyan, J.G. (1999) Polymorphism in silica studied in the local density and generalized-gradient approximations. Journal of Physics: Condensed Matter, 11, 3833–3874.

Downs, J.W. (1995) Electron density and electrostatic potential of coesite. The Journal of Physical Chemistry, 99, 6849–6856.

Downs, J.W. and Swope, R.J. (1992) The Laplacian of the electron density and the electrostatic potential of danburite, $CaB_2Si_2O_8$. The Journal of Physical Chemistry, 96, 4834–4840.

Downs, R.T. and Palmer, D.C. (1994) The pressure behavior of α-cristobalite. American Mineralogist, 79, 9–14.

Du, M.H., Kolchin, A., and Cheng, H.P. (2003) Water-silica surface interactions: A combined quantum-classical molecular dynamic study of energetics and reaction pathways. Journal of Chemical Physics, 119, 6418–6422.

Feth, S., Gibbs, G.V., Boisen, M.B., and Myers, R.H. (1993) Promolecule radii for nitrides, oxides, and sulfides—A comparison with effective ionic and crystal radii. Journal of Physical Chemistry, 97, 11445–11450.

Feynman, R.P. (1939) Forces in molecules. Physical Review, 56, 340–343.

Gatti, C. (2005) Chemical bonding in crystals: New directions. Zeitschrift für Kristallographie, 220, 399–457.

Geisinger, K.L. and Gibbs, G.V. (1981) SiSSi and SiOSi bonds in molecules and solids: A comparison. Physics and Chemistry of Minerals, 7, 204–210.

Gibbs, G.V. (1982) Molecules as models for bonding in silicates. American Mineralogist, 67, 421–450.

Gibbs, G.V., Prewitt, C.T., and Baldwin, K.J. (1977) A study of the structural chemistry of coesite. Zeitschrift für Kristallographie, 145, 108–123.

Gibbs, G.V., Spackman, M.A., and Boisen Jr., M.B. (1992) Bonded and promolecule radii for molecules and crystals. American Mineralogist, 77, 741–750.

Gibbs, G.V., Downs, J.W., and Boisen Jr., M.B. (1994) The elusive SiO bond. In P.J. Heaney, C.T. Prewitt, and G.V. Gibbs, Eds., Silica: Physical Behavior, Geochemistry, and Materials Applications, 29, p. 331–68. Reviews in Mineralogy, Mineralogical Society of America, Chantilly, Virginia.

Gibbs, G.V., Hill, F.C., and Boisen Jr., M.B. (1997) The SiO bond and electron density distributions. Physics and Chemistry of Minerals, 24, 167–178.

Gibbs, G.V., Boisen Jr., M.B., Hill, F.C., Tamada, O., and Downs, R.T. (1998) SiO and GeO bonded interactions as inferred from the bond critical point properties of electron density distributions. Physics and Chemistry of Minerals, 25, 574–584.

Gibbs, G.V., Rosso, K.M., Teter, D.M., Boisen Jr., M.B., and Bukowinski, M.S.T. (1999) Model structures and properties of the electron density distribution for low quartz at pressure: a study of the SiO bond. Journal of Molecular Structure, 485–486, 13–25.

Gibbs, G.V., Boisen, M.B., Rosso, K.M., Teter, D.M., and Bukowinski, M.S.T. (2000) Model structures and electron density distributions for the silica polymorph coesite at pressure: An assessment of OO bonded interactions. Journal of Physical Chemistry B, 104, 10534–10542.

Gibbs, G.V., Boisen, M.B., Beverly, L.L., and Rosso, K.M. (2001) A computational quantum chemical study of the bonded interactions in earth materials and structurally and chemically related molecules. In R.T. Cygan and J.D. Kubicki, Eds., Molecular Modeling Theory: Applications in the Geosciences, 42, p. 345–381. Reviews in Minerology and Geochemistry, Mineralogical Society of America, Chantilly, Virginia.

Gibbs, G.V., Cox, D.F., Boisen, M.B., Downs, R.T., and Ross, N.L. (2003a) The electron localization function: a tool for locating favorable proton docking sites in the silica polymorphs. Physics and Chemistry of Minerals, 30, 305–316.

Gibbs, G.V., Whitten, A.E., Spackman, M.A., Stimpfl, M., Downs, R.T., and Carducci, M.D. (2003b) An exploration of theoretical and experimental electron density distributions and SiO bonded interactions for the silica polymorph coesite. Journal of Physical Chemistry B, 107, 12996–13006.

Gibbs, G.V., Cox, D.F., and Rosso, K.M. (2004) A connection between empirical bond strength and the accumulation of the electron density at the bond critical points of the Si-O bonds in silicates. Journal of Physical Chemistry B, 108, 7643–7645.

Gibbs, G.V., Cox, D.F., Ross, N.L., Crawford, T.D., Burt, J.B., and Rosso, K.M. (2005a) A mapping of the electron localization function for earth materials, Physics and Chemistry of Minerals, 32, 208–221.

Gibbs, G.V., Downs, R.T., Prewitt, C.T., Rosso, K.M., Ross, N.L., and Cox, D.F. (2005b) Electron density distributions calculated for the nickel sulfides millerite, vaesite, and heazlewoodite and nickel metal: A case for the importance of Ni-Ni bond paths for electron transport. Journal of Physical Chemistry B, 109, 21788–21795.

Gibbs, G.V., Jayatilaka, D., Spackman, M.A., Cox, D.F., and Rosso, K.M. (2006a) Si-O Bonded interactions in silicate crystals and molecules: A comparison. Journal of Physical Chemistry A, 110, 12678–12683.

Gibbs, G.V., Spackman, M.A., Jayatilaka, D., Rosso, K.M., and Cox, D.F. (2006b) Bond length and local energy density property connections for non-transition-metal oxide-bonded interactions. Journal of Physical Chemistry A, 110, 12259–12266.

Gibbs, G.V., Cox, D.F., Rosso, K.M., Ross, N.L., Downs, R.T., and Spackman, M.A. (2007) Theoretical electron density distributions for Fe- and Cu-sulfide Earth materials: A connection between bond length, bond critical point properties, local energy densities and bonded interactions. Journal of Physical Chemistry B, 111, 1923–1931.

Gibbs, G.V., Downs, R.T., Cox, D.F., Ross, N.L., Prewitt, C.T., Rosso, K.M., Lippmann, T., and Kirfel, A. (2008a) Bonded interactions and the crystal chemistry of minerals: A review. Zeitschrift für Kristallographie, 223, 1–40.

Gibbs, G.V., Downs, R.T., Cox, D.F., Rosso, K.M., Ross, N.L., Kirfel, A., Lippmann, T., Morgenroth, W., and Crawford, T.D. (2008b) Experimental bond

critical point and local energy density properties determined for Mn-O, Fe-O, and Co-O bonded interactions for tephroite, Mn_2SiO_4, fayalite, Fe_2SiO_4, and Co_2SiO_4 olivine and selected organic metal complexes: Comparison with properties calculated for non-transition and transition metal M-O bonded interactions for silicates and oxides. Journal of Physical Chemistry A, 112, 8811–8823.

Gibbs, G.V., Wallace, A.F., Cox, D.F., Dove, P.M., Downs, R.T., Ross, N.L., and Rosso, K.M. (2009) Role of directed van der Waals bonded interactions in the determination of the structures of molecular arsenate solids. The Journal of Physical Chemistry A, 113, 736–749.

Gillespie, R.J. and Johnson, S.A. (1997) Study of bond angles and bond lengths in disiloxane and related molecules in terms of the topology of the electron density and its Laplacian. Inorganic Chemistry, 36, 3031–3039.

Guerra, C.F., Handgraaf, J.W., Baerends, E.J., and Bickelhaupt, F.M. (2004) Voronoi deformation density (VDD) charges: Assessment of the Mulliken, Bader, Hirshfeld, Weinhold, and VDD methods for charge analysis. Journal of Computational Chemistry, 25, 189–210.

Haaland, A., Helgaker, T.U., Ruud, K., and Shorokhov, D.J. (2000) Should gaseous BF_3 and SiF_4 be described as ionic compounds? Journal of Chemical Education, 77, 1076–1080.

Hansen, N.K. and Coppens, P. (1978) Electron population analysis of accurate diffraction data 6. Testing aspherical atom refinements on small-molecule data sets. Acta Crystallographica Section A, 34, 909–921.

Harrison, W.A. (1978) Is silicon dioxide covalent or ionic? In S.T. Pantelides, Ed., The Physics of SiO_2 and its Interfaces, p. 105, Chapter 2. Pergamon Press, New York.

Hill, R.J., Newton, M.D., and Gibbs, G.V. (1983) A crystal chemical study of stishovite. Journal of Solid State Chemistry, 47, 185–200.

Hoffmann, R. (1988) Solids and Surfaces: A Chemist's View of Bonding in Extended Structures, 142 p. VCH Publishers, New York.

Ida, Y. (1976) Interionic repulsive force and compressibility of ions. Physics of the Earth and Planetary Interiors, 13, 97–104.

Jackson, M.D. and Gibbs, G.V. (1988) A modeling of the coesite and feldspar framework structure types of silica as a function of pressure using modified electron-gas methods. Journal of Physical Chemistry, 92, 540–545.

Jackson, M.D. and Gordon, R.G. (1988) MEG investigation of low pressure silica—Shell model for polarization. Physics and Chemistry of Minerals, 16, 212–220.

Kihara, K. (1990) An X-ray study of the temperature-dependence of the quartz structure. European Journal of Mineralogy, 2, 63–77.

Kirfel, A., Krane, H.G., Blaha, P., Schwarz, K., and Lippmann, T. (2001) Electron-density distribution in stishovite, SiO_2: A new high-energy synchrotron-radiation study. Acta Crystallographica Section A, 57, 663–677.

Koch-Muller, M., Fei, Y., Hauri, E., and Liu, Z. (2001) Location and quantitative analysis of OH in coesite. Physics and Chemistry of Minerals, 28, 693–705.

Kuntzinger, S., Ghermani, N.E., Dusausoy, Y., and Lecomte, C. (1998) Distribution and topology of the electron density in an aluminosilicate compound from high-resolution X-ray diffraction data: the case of scolecite. Acta Crystallographica Section B: Structural Science, 54, 819–833.

Lasaga, A.C. and Gibbs, G.V. (1990) Ab initio quantum-mechanical calculations of water-rock interactions—Adsorption and hydrolysis reactions. American Journal of Science, 290, 263–295.

Levien, L. and Prewitt, C.T. (1981) High-pressure crystal-structure and compressibility of coesite. American Mineralogist, 66, 324–333.

Levien, L., Prewitt, C.T., and Weidner, D.J. (1980) Structure and elastic properties of quartz at pressure. American Mineralogist, 65, 920–930.

Lieb, E.H. and Loss, M. (1997) Analysis, 271 p. American Mathematical Society, Providence, Rhode Island.

Marsden, J.E. and Tromba, A. (1976) Vector Calculus, 449 p. W.H. Freeman and Co., San Francisco.

Matsui, Y., Kawamura, K., and Syono, Y. (1982) Molecular dynamic calculations applied to silicates: Molton and vitreous $MgSiO_3$ and Mg_2SiO_4 under low and high pressure. In S. Akimoto and M.H. Manghnani, Eds., High-Pressure Research in Geophysics, 12, p. 433–438. Advances in Earth and Planetary Sciences, Center for Academic Publications Japan, Tokyo; Reidel, Boston.

Mendeleeff, D. (1889) LXIII.—The periodic law of the chemical elements. Journal of the Chemical Society, Transactions, 55, 634–656.

Miyamoto, M. and Takeda, H. (1980) An interpretation of the structure of mantle minerals at high pressures. Geochemical Journal, 243–248.

Nangia, S. and Garrison, B.J. (2008) Reaction rates and dissolution mechanisms of quartz as a function of pH. Journal of Physical Chemistry A, 112, 2027–2033.

O'Keeffe, M. and Hyde, B.G. (1976) Cristobalites and topologically-related structures. Acta Crystallographica Section B, 32, 2923–2936.

——— (1981) The role of nonbonded forces in crystals. In M. O'Keeffe and A. Navrotsky, Eds., Structure and Bonding in Crystals, 1, p. 222–254. Academic Press, New York.

O'Keeffe, M. and McMillan, P.F. (1986) The silicon-oxygen-silicon force field: ab initio MO calculations. Journal of Physical Chemistry, 90, 541–542.

Panero, W.R. and Stixrude L.P. (2004) Hydrogen incorporation in stishovite at high pressures and symmetric hydrogen bonding in δ-AlOH. Earth and Planetary Letters, 221, 421–431.

Parr, R.G. and Yang, W. (1989) Density-Functional Theory of Atoms and Molecules, 333 p. Oxford University Press, U.K.

Pauling, L. (1929) The principles determining the crystal structure of complex ionic crystals. Journal of the American Chemical Society, 51, 1010–1026.

——— (1931) The nature of the chemical bond. II. The one-electron bond and the three-electron bond. Journal of the American Chemical Society, 53, 3225–3237.

——— (1939) The Nature of the Chemical Bond. Cornell University Press, Ithaca, New York.

Pelmenschikov, A., Strandh, H., Pettersson, L.G.M., and Leszczynski, J. (2000) Lattice resistance to hydrolysis of Si-O-Si bonds of silicate minerals: Ab initio calculations of a single water attack onto the (001) and (111) beta-cristobalite surfaces. Journal of Physical Chemistry B, 104, 5779–5783.

Pendas, A.M., Francisco, E., Blanco, M.A., and Gatti, C. (2007) Bond paths as privileged exchange channels. Chemistry—A European Journal, 13, 9362–9371.

Phillips, J.C. (1970) Ionicity of the chemical bond in crystals. Reviews of Modern Physics, 42, 317–356.

Prewitt, C.T. (1985) Crystal chemistry: Past, present, and future. American Mineralogist, 70, 443–454.

Prencipe, M. and Nestola, F. (2007) Minerals at high pressure. Mechanics of compression from quantum mechanical calculations in a case study: the beryl ($Al_4Be_6Si_{12}O_{36}$). Physics and Chemistry of Minerals, 30, 471–479.

Prencipe, M., Tribaudino, M., and Nestola, F. (2002) Charge density analysis of spodumene ($LiAlSi_2O_6$) from ab initio Hartree-Fock calculations. Physics and Chemistry of Minerals, 30, 606–614.

Rosso, K.M., Gibbs, G.V., and Boisen, M.B. (1999) SiO bonded interactions in coesite: a comparison of crystalline, molecular, and experimental electron density distributions. Physics and Chemistry of Minerals, 26, 264–272.

Runtz, G.R., Bader, R.F.W., and Messer, R.R. (1977) Definition of bond paths and bond directions in terms of molecular charge-distribution. Canadian Journal of Chemistry—Revue Canadienne De Chimie, 55, 3040–3045.

Sanders, M.J., Leslie, M., and Catlow, C.R.A. (1984) Interatomic potentials for SiO_2. Journal of the Chemical Society, Chemical Communications, 1271–1273.

Shannon, R.D. and Prewitt, C.T. (1969) Effective ionic radii in oxides and fluorides. Acta Crystallographica, B25, 925–946.

Slater, J.C. (1964) Atomic radii in crystals. Journal of Chemical Physics, 41, 3199–3204.

Smyth, J.R. (1989) Electrostatic characterization of oxygen sites in minerals. Geochimica et Cosmochimica Acta, 53, 1101–1110.

——— (2006) Hydrogen in high pressure silicate and oxide mineral structures. In H. Keppler and J.R. Smyth, Eds., Water in Nominally Anhydrous Minerals, 62, p. 85–115. Reviews in Mineralogy and Geochemistry, Chantilly, Virginia.

Spackman, M.A. and Maslen, E.N. (1985) Electron density and the chemical bond. A reappraisal of Berlin's theorem. Acta Crystallographica Section A, 41, 347–353.

Stewart, R. (1976) Electron population analysis with rigid pseudoatoms. Acta Crystallographica Section A, 32, 565–574.

Stewart, R.F., Whitehead, M.A., and Donnay, G. (1980) The ionicity of the Si-O bond in low quartz. American Mineralogist, 65, 324–326.

Stewart, R.F., Spackman, M.A., and Flensburg, C. (2000) VALRAY User's Manual. Carnegie Mellon University, Pittsburgh; University of Copenhagen, Denmark.

Teter, D.M., Gibbs, G.V., Boisen, M.B., Allan, D.C., and Teter, M.P. (1995) First-principles study of several hypothetical silica framework structures. Physical Review B, 52, 8064–8073.

Tsirelson, V.G. (2002) The mapping of electronic energy distributions using experimental electron density. Acta Crystallographica Section B, Structural Science, 58, 632–639.

Vempati, C.S. and Jacobs, P.W.M. (1983) Crystal potentials for alpha-quartz. Radiation Effects and Defects in Solids, 73, 285–289.

Wojdel, J.C., Zwijnenburg, M.A., and Bromley, S.T. (2006) Magic silica clusters as nanoscale building units for super-(tris)tetrahedral materials. Chemistry of Materials, 18, 1464–1669.

Woodley, S.M. and Catlow, R. (2008) Crystal structure prediction from first principles. Nature Materials, 7, 937–946.

Zwijnenburg, M.A., Bromley, S.T., Alsenoy, C.V., and Maschmeyer, T. (2002) Factors affecting ionicity in all-silica materials: A density functional cluster study. Journal of Physical Chemistry A, 106, 12376–12385.

Manuscript received February 9, 2009
Manuscript accepted April 23, 2009
Manuscript handled by G. Diego Gatta